Surface and 2D magnetism

1992 J. Phys.: Condens. Matter 4 8395

(http://iopscience.iop.org/0953-8984/4/44/004)

J. Phys.: Condens. Matter 4 (1992) 8395–8434. Printed in the UK

REVIEW ARTICLE

Surface and 2D magnetism

H C Siegmann

Swiss Federal Institute of Technology, Zurich, Switzerland

Received 14 April 1992, in final form 2 September 1992

Abstract. The development of surface science and specifically of spin-polarized electron spectroscopy has been the driving force for a new era of surface and 2D magnetism. Classical primary magnetic quantities such as the temperature dependence of the spontaneous magnetization, the Curie point, the magnetic anisotropies, the variation of the quantum mechanical exchange interaction at clean or modified surfaces, and special surface-induced magnetic structures can now be determined with spin-polarized electron spectroscopies. But a variety of new fields are also appearing, for instance ultrafast time-resloved magnetometry employing laser-induced photoemission of spin-polarized electrons, and imaging of magnetic domains with unprecedented spatial resolution via spin-polarized cascade electrons. Furthermore, by analysing the spin of the photoemitted electrons or by observing the Bremsstrahlung emitted when a spin-polarized electron beam strikes the surface, the majority- and minority-spin electron states in ferromagnets can be investigated separately. Three types of spin-split electron state appear at the surface of a ferromagnet: the bulk magnetic bands, the surface states of Schottky type, and the image potential surface states.

With ultrathin ferromagnetic films, magnetometry employing the measurement of the spin polarization of low-energy cascade electrons produces magnificent images of the magnetic domains and reveals the conditions for their occurrence. The dramatic response of the spontaneous magnetization to external disturbances such as an applied magnetic field or an exchange field transferred from a substrate is also obtained. The critical phenomena observed in surface and 2D magnetism fit well into the framework set by the theory many years ago, while the theoretically predicted exotic 2D ferromagnetism in elements that do not exhibit magnetism in 3D has not yet been verified beyond doubt.

Contents

0953-8984/92/448395+40$07.50

1. Basic questions and experimental methods

Magnetism has been studied since the beginning of our civilization and so much multifacetted information has been gathered that one single person can no longer write a review surveying all that is important. Surface science, itself very young, has brought into being within 20 years the new field of surface and 2D (two-dimensional) magnetism. It is quite obvious that surface and 2D magnetism will be a gigantic field by itself very soon.

Almost every possible physical property changes when a surface or a thin film becomes magnetic: the electronic structure, the crystal structure, and with it optical reflection, photoelectric properties, the hyperfine fields, thermal and electric conduction to name but a few. The quantity of central interest in magnetism is of course the magnetization M which is defined as the magnetic moment/volume:

$$M = n_A n_B \mu_B \tag{1}$$

where n_A is the density of atoms and n_B the number of Bohr magnetons μ_B carried by each atom. The occurrence of the magnetization is a manifestation of one of the most significant discoveries of our century, the indistinguishability of the electrons. It leads to the exchange degeneracy, on the basis of which the exchange interaction can be qualitatively explained.

Experimentally, one has to determine $M(H, T)$ for each atomic layer at the surface, or in a thin film, as it depends on the external magnetic field H and on the temperature T. From $M(H, T)$ one obtains the spontaneous magnetization $M_0(T)$ which is generated in the absence of an external field by the quantum mechanical exchange interaction within one single Weiss domain. The temperature at which M_0 vanishes is the Curie point T_C. Very general theoretical arguments predict how M_0 should vary at low temperatures $T/T_C \leqslant 0.3$ and with which 'critical exponent' M_0 should vanish as $T/T_C \to 1$ [1, 2].

Magnetometry at surfaces and in thin films poses great challenges. As a precondition of any measurement, it requires structural and chemical definition of the often complex magnetic materials on an atomic scale. This implies generally that the most advanced ultrahigh-vacuum techniques and surface-sensitive sample characterization must be developed in addition to solving the problem of how to get a grip on the local magnetization in the surface layers. The basic questions in surface magnetism can be summarized as follows.

(i) What is the magnetic moment of the atoms at the surface? Any changes in the occupancy of electronic states at the surface must produce a change of the surface magnetic moment. Theoretical studies have indicated that band narrowing

and surface states can also lead to further significant changes in surface magnetic moments.

(ii) What is the magnetic coupling of the surface atoms? It is well known that the extent and shape of the wavefunctions of surface atoms are different from those of the bulk atoms. This leads to a different overlap between neighbouring atoms and is bound to affect the quantum mechanical exchange interaction severely.

(iii) What are the magnetic anisotropies at the surface? The occurrence of magnetic anisotropies is due to the spin–orbit interaction. In the bulk of 3d transition metals, the orbital moment is small because it is largely quenched in the crystal field. Consequently, the spin–orbit coupling and the resulting magnetic anisotropy are small in the bulk except with 4f materials. At the surface, the symmetry of the crystal is broken. Therefore, the orbital moment is quenched to a lesser extent which may result in very large surface-induced magnetic anisotropies.

For ultrathin films on non-magnetic substrates, the new prototypes of 2D magnetism, the questions on M_0, the exchange interaction and the anisotropy remain the same, yet there are additional fundamental issues concerning the influence of the crystal structure of the substrate enforced on the epitaxial magnetic overlayer and the conditions for continuous phase transitions in 2D bodies. These questions have generated an impressive amount of activity in magnetism which has led to the discovery of some striking new magnetic phenomena like long-range interactions and giant magnetoresistance in coupled films. These phenomena in turn provide a new basis for the theory as well as for the applications.

Theoretical work is essential in recognizing and formulating the basic questions, yet it has not been able to produce reliable answers even for the case of model systems like Fe and Ni [1]. Hence the main focus is with trying to find experimental answers. The experimental results have been obtained with a wide variety of techniques including Josephson magnetometry, Mössbauer spectroscopy, the magneto-optic Kerr effect and the Faraday effect, Brillouin light scattering, electron spin resonance, and the elastic and inelastic scattering, photoemission and capture of spin-polarized electrons. One has to find a path through the maze of various results obtained on the extremely delicate magnetic systems. Furthermore, it is important to evaluate how the signal obtained with newly developed and sometimes exotic methods relates to the primary magnetic properties, namely the spontaneous magnetization M_0, the Curie point T_C and the magnetic anisotropy constants. The experimental methods can be classified as follows:

(i) induction, torque and force magnetometry;

(ii) experiments which rely on the spin–orbit energy to couple polarized light to the magnetization;

(iii) experiments which measure the hyperfine field;

(iv) experiments which probe the electron spin polarization.

So far, most of the results have been obtained by spin-polarized electron spectroscopies. Therefore, a thorough discussion of magnetometry with spin-polarized electrons is appropriate. However, results obtained with other methods will also be included.

1.1. Magnetic information from measurement of electron spin polarization or spin asymmetry

First, one needs to discuss the question of what information on $M(H, T)$ may be

obtained with spin-polarized electron beam techniques. In these techniques, electrons are extracted from the sample surface and emitted into the vacuum. These electrons are then focused into a beam and the spin polarization P of the beam is measured, usually in a scattering experiment [3]. It will be shown below that P can be directly related in most cases to the magnetization M within the surface layers. It is, however, important to be aware of the complexities that may arise.

The vector of the spin polarization is defined as $P = \{\langle\sigma_x\rangle, \langle\sigma_y, \langle\sigma_z\rangle\}$ where $\langle\sigma_v\rangle$ are expectation values of the spin direction along the three coordinates; the definition is meaningful in the non-relativistic limit which applies to the experiments discussed here. We have $|P| = (n^{\uparrow} - n^{\downarrow})/(n^{\uparrow} + n^{\downarrow}) \leqslant 1$ where $n^{\uparrow}(n^{\downarrow})$ is the density of spin-up (spin-down) electrons in the beam. It should be noted that the experiment can also be inverted: first, a beam of spin-polarized electrons is formed, for instance with a spin-polarized GaAs electron source, and the emission of light or scattered electrons is measured when the spin-polarized electron beam strikes the solid. The dependence of the light or electron emission on the direction of the spin polarization of the incident beam is called the spin asymmetry A. It provides the relevant information in the inverted experiment [4].

P should directly reflect that part of the magnetization M which is generated by spontaneous alignment of the electron spins in the surface. This arises because conservation of spin is the dominant rule in most processes of electron emission, and because the escape depth of electrons is very short. The orbital part of M will not contribute to P as it disappears in the process of electron emission and beam formation. At the surface, the crystal field is generally distorted which may lead to relatively large changes of the orbital moment compared to bulk material. Therefore, it is important to keep in mind that P obtained in electron beam techniques accounts only for the spin part M_σ of the magnetization. This yields

$$P = fM_\sigma/(n_e n_A \mu_B) \tag{2}$$

where f is a dimensionless function discussed below, and n_e the total number of electrons in the open shells of the atoms. In the following, we will omit the index σ for simplicity. Induction, torque and force magnetometers determine of course the total magnetization including the orbital part.

The factor f in equation (2) cannot be generally predicted. The amount and origin of the electrons emitted from any surface depends on how the energy is supplied to induce electron emission. The most common source of energy is photons or primary electrons, that is one has photoemission or secondary electron emission. In photoemission for example, the energy, polarization and angle of incidence of the photons determines the relative probability of electron emission from the various electron states in the solid. Hence, the contribution of each type of electron state to the total electron beam is variable. Therefore, the polarization of the emitted electron beam does not represent the same average as the polarization of electrons in equilibrium within the solid.

One basic assumption is that P and M are collinear as postulated in equation (2). This is founded on the general quantum mechanical result that once the quantization axis is fixed by the direction of the total magnetization M, the spin polarization of the electrons must be collinear, either parallel or antiparallel to M. However, this is applicable strictly only to the case of highly symmetric objects such as atoms. In solids, the scattering on selected crystal planes or the crystal structure itself can define

a new quantization axis which might destroy the collinearity of P and M. In the design of a magnetometer based on spin-polarized electrons one has to take care that such complications are absent and that P is either antiparallel or parallel to M. The fact that P can have either sign with respect to M is best explained with the example of ferromagnetic Ni, where the electrons close to the Fermi level E_F are polarized opposite to the average spin polarization. Hence if the electron emission conditions favour states at E_F, the observed polarization changes sign. Similarly, if one has a ferrimagnet with two opposite sublattice magnetizations M_A and M_B, electron emission can occur predominantly from sublattice A or from B, and the sign of P will change accordingly while the total magnetization $M = M_A + M_B$ remains fixed. However, if the conditions of electron emission are kept constant, P must change sign when M changes sign. This leads to

$$P = C_1 M_\sigma + C_2 M_\sigma^3 + C_3 M_\sigma^5 + \dots \tag{3}$$

where $C_1, C_2, \dots$ are constants. Equation (3) shows that P is proportional to M_σ if the changes of M_σ are not large. Non-linear phenomena affecting the proportionality include multiple spin-dependent scattering of electrons in the emission process and, in an energy-resolved electron emission experiment, energy shifts of spectral features that can occur when the temperature T changes. In summary, the following general statements apply.

(i) absolute magnetometry is not yet possible in spin-polarized electron beam experiments. However, with photons of very high energy, one might be able to suppress the scattering phenomena discussed in section 1.2. Therefore, absolute magnetometry could become possible with future synchrotron radiation sources. Møller scattering of high-energy spin-polarized electrons is one existing example of absolute magnetometry frequently used in high-energy physics [5].

(ii) P and M are collinear under appropriate experimental conditions. Therefore, magnetic structures, e.g., in domain walls, or magnetic hysteresis loops including magnetic remanence and coercivity, may be determined by measuring P.

(iii) P and M are proportional in many cases, particularly if M is small or if only small changes of M are considered. This means that one can determine the T-dependence of M_0 by measuring $P(T)$ in the spin-wave regime where the changes of M_0 are small. Similarly, close to T_C, M is small and the critical behaviour of M_0 as well as T_C can be determined from $P(T)$.

Magnetometry with spin-polarized electrons offers the following special features which have added some new and exciting topics to magnetism [6].

(i) *Time resolution.* Pulsed lasers or synchrotron light sources provide short photon pulses. With such a pulse, enough photoelectrons can be emitted from a surface to perform an accurate measurement of P yielding the magnetization averaged over the light pulse duration. This is typically of the order of 10^{-11} s, hence orders of magnitude shorter than in conventional magnetometry. The pulse of photoemitted electrons is space charge limited, but this does not affect P as the spin of the total bunch of emitted electrons must be conserved.

(ii) *Spatial resolution.* A primary electron beam may be focused into an extremely small spot at the surface. Secondary electrons are emitted from the close neighbourhood of the focus, and their polarization can be measured. The lateral resolution is sufficient in some favourable cases to measure directly the spontaneous

polarization within one domain without applying an external field. Unique images of magnetic domains and the internal structure of domain walls are also obtained with this technique when used in a scanning mode.

(iii) *Element specificity*. Electrons excited from preselected atomic shells yield a measure of the local magnetization in the atom from which they are emitted. This is critical in ascertaining the contribution of each element in a magnetic alloy or from nearest-neighbour atoms in the form of overlayers or substrate layers.

(iv) *Magnetization of specific electron states*. Spin-polarized electron spectroscopies permit selection of electrons emitted from specific states and determine their contribution to the total magnetization. This helps to develop the theory of metallic magnetism. Furthermore, it shows which electron states are modified by the interface or by chemical reactions.

(v) *Magnetism in unoccupied or fully occupied electron states*. Unoccupied or fully occupied states do not contribute to the magnetization, yet may undergo Zeeman splitting in the exchange field. Spin-polarized electron beam techniques are the most direct way to investigate this splitting in the various electron states [7, 8].

1.2. Magnetometry with low-energy spin-polarized electrons

Metal surfaces emit copious amounts of low-energy electrons when irradiated with a primary beam of electrons. These low-energy secondary electrons or cascade electrons turn out to be of great value for magnetometry. The cascade electrons are created by inelastic scattering events in which electrons from states at and below the Fermi energy are excited to an escape level above the vacuum energy. The establishment of an equilibrium distribution of the cascade electrons at energies $\leqslant 10$ eV requires a characteristic time τ, which is given by the average lifetime of the electrons in the excited states. τ can also be translated into a characteristic length λ via the group velocity of the electrons in the excited states over which the electron cascade is formed. λ in turn is the probing depth from the surface over which specific electronic properties of the metal can be sampled by spectroscopic analysis of energy, angular distribution, and spin polarization P_C of the cascade electrons. A large amount of data for λ has been accumulated from the overlayer method, where the attenuation of a prominent substrate feature is measured as a function of the overlayer thickness d and fitted with an exponential decay $\exp(-d/\lambda)$. The data for many materials are often displayed as a 'universal curve' which shows λ as a function of energy E [9]. Measurements of P_C have, however, clearly established that λ is much shorter at $E < 40$ eV than expected from the universal curve and has a pronounced material dependence. The polarization P_C of the cascade at $E < 10$ eV is enhanced by a factor ~ 2 compared to the spin polarization P_i of the secondaries at higher energies ($E > 10$ eV). Apart from features due to Auger processes and the spin-polarized band structure above the vacuum level, P_i is equal to the initial spin polarization in thermal equilibrium as determined on bulk samples with conventional magnetometry. The enhancement $f \simeq 2$ in equation (2) of P_C turns out to be closely connected to the short λ or the strong inelastic scattering cross section of low-energy electrons in a transition metal, as will be shown below.

A well-defined magnetization profile can be constructed at a surface prepared by molecular beam epitaxy of, e.g. BCC Fe(100) on the Au(100) surface. Taborelli [10] has measured the polarization of the cascade electrons produced by a 3 keV primary electron beam as a function of the number of Fe overlayers for this system. He found that P_C was substantial with one monolayer of Fe and increased almost to its

limiting value with the deposition of only three monolayers of Fe. This observation has a simple interpretation if λ is small, but can be reconciled with a large λ if a spin-filtering process exists in the magnetic overlayer which reduces the transmission of low-energy spin-down electrons and creates more spin-up electrons. Abraham and Hopster [11] have proposed, based on their impressive high-resolution spin-polarized electron energy loss studies on Ni, that Stoner excitations [12] provide a mechanism for such a spin filtering. This and similar experiments on Fe [13] yield only the differential cross section for Stoner excitations. The total cross section for these excitations, however, is not currently known with sufficient accuracy to permit a qualitative evaluation of the effect on P_C. In addition, the question remains of whether the short probing depth for spin-polarized electrons from ferromagnets is only a magnetic probing depth or a probing depth of low-energy electrons in general.

Gokhale and Mills have proposed still another explanation for the enhancement of P_C over P_i. They maintain that elastic scattering of the electrons on the Fe atoms, which also is spin dependent, is responsible for it [14].

The answer to these questions comes from depositing a *non-magnetic* overlayer on top of a magnetic substrate and measuring P_C as a function of the thickness of the overlayer [15, 16]. As the overlayer is non-magnetic, there cannot be preferential scattering of one particular spin state within this overlayer. It turns out that λ obtained for non-magnetic transition metals is equally as short as in magnetic overlayers. Paul *et al* [17] have generated a layer of non-magnetic Fe* by depositing a layer of Ta on the surface. It turns out that λ^* of Fe* is the same as λ in ferromagnetic Fe. Hence Stoner excitations or any excitations involving a spin flip are not important in the formation of the cascade. In other words, the mean free path for conservation of spin is larger than the one for conservation of energy. Compilation of the available data obtained from P_C analysis valid for electron energies within ~ 2 eV from threshold with transition metals proves that there is still a universal behaviour irrespective of whether a metal is ferromagnetic or not. Figure 1 shows $1/\lambda$ for Au [17], Ag [18], Ni [15], Fe [17, 19], Cr [20, 18], Ta [16, 17] and Gd [17] versus the number of holes in the d band. Note that each d state can accommodate two electrons. For the ferromagnetic metals, the average number of spin-up and spin-down holes is plotted. For the non-magnetic metals the d holes were determined from the atomic configuration. We see that $1/\lambda$, which is proportional to the inelastic scattering cross section, is simply proportional to the number of holes in the d band. The much improved quality of the data reflects the fact that one has learned to avoid the pitfalls of the overlayer method such as island formation and interdiffusion. It also shows the accuracy inherent in the analysis of P_C.

With these experimental advances it is clear that the golden rule or the random k-approximation is sufficient for understanding the cascade formation in transition metals. The number of electrons lost by scattering is then simply proportional to the number of available unoccupied states. Cu could be exceptional as the inelastic mean free path found in [15] is much shorter than in Ag and Au. More experiments are necessary to decide whether Cu is a special case amongst the noble metals. A short λ was also found for Cs [17], which should have a large λ as well as there are no d holes close to E_F. Yet with Cs it is obvious that it is the plasmon of exceptionally low energy that reduces λ of low-energy electrons.

As the number of holes is spin dependent in ferromagnets, λ becomes spin dependent as demonstrated clearly in [19]. Figure 1 shows the average λ only. It is straightforward to calculate the enhancement factor f in equation (2) of P_C

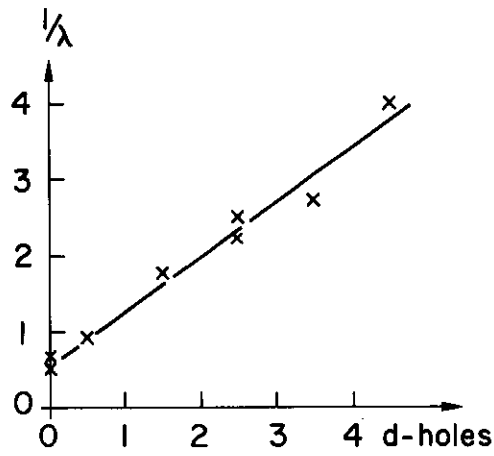

Figure 1. Number of holes $(5-n)$ in the d band versus inverse attenuation length $1/\lambda$ (nm^{-1}) for cascade electrons close to threshold, for (from left to right) Au, Ag, Ni, Fe, Cr (two data points), Ta and Gd. With ferromagnetic metals, the spin-averaged λ is plotted, and with Cr, Ta and Gd the number n of d electrons is taken from the atomic configuration.

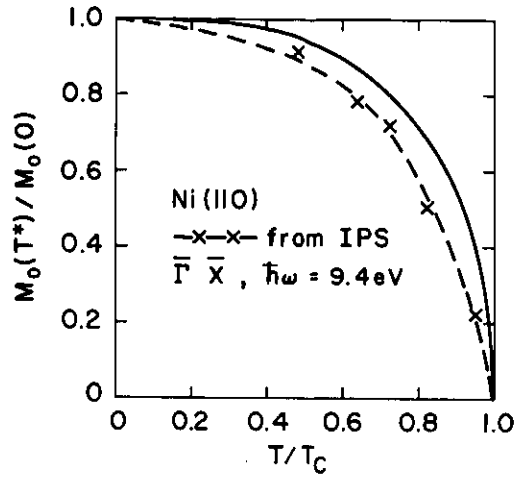

Figure 2. Brillouin function for spin $\frac{1}{2}$ (full line) to represent the thermal decrease of the bulk magnetization in Ni. The data points are calculated according to equation (6) from the experiments in [21]. They represent the partial magnetization of the 3d bands in Ni along the $\bar{\Gamma}\bar{X}$ direction as observed in inverse photoemission (IPS). The dashed line is the relative spin polarization $P_C(T^*)/P_C(0)$ observed with low-energy secondary electrons on Ni(110) for instance in [23].

over P_i. The number of electrons excited from the occupied part of the d band is $\alpha(n \pm \Delta n)$, where α is the excitation probability, n number of d electrons and $\pm\Delta n$ the increase (decrease) of the spin-up (spin-down) d electrons when the magnetization is generated. $(n+\Delta n)$ is then the number of spin-up electrons in the ferromagnetic state.

The loss of electrons by inelastic scattering is $\alpha(n+\Delta n)-\beta\alpha(n+\Delta n)(5-(n+\Delta n))$. 5 is the total number of d states, $5-(n+\Delta n)$ the number of majority holes, and β the transition probability for de-excitation. The current of spin-up electrons emerging from the surface is then $i^{\uparrow} = \alpha(n+\Delta n)\{1-\beta(5-(n+\Delta n))\}$. Similarly, the current of spin-down electrons is given by $i^{\downarrow} = \alpha(n-\Delta n)\{1-\beta(5-(n-\Delta n))\}$. With $P_i = \Delta n/n$, the polarization of the cascade is given by

$$P_C = f P_i = \{1+\beta(2n-5)\}/\{1+\beta((P_i^2+1)n-5)\}P_i. \qquad (4)$$

We see that the de-excitation strength β determines the enhancement factor f: $f=1$ if $\beta = 0$. The enhancement is not due to spin flips which is seen from equation (4) by putting $P_i = \pm 1$, which yields $f = 1$; that is, no enhancement occurs if only either one of the spin states is present. Finally, it is obvious that P_C is not proportional to the magnetization M, compare equation (2), as f contains P_i^2 in the denominator. However, equation (4) is obviously consistent with equation (3) and C_2 can now be calculated. It turns out that C_2 is sufficiently small for most applications. In the most unfavourable case of Fe, $n \simeq 3.5$, $\Delta n \simeq 1$, $P_i = 0.286$. With $\beta = 0.2$, equation (4) yields $f = 1.85$ close to the observations. If T increases such that

$\Delta P_i(T)/P_i(0) = 0.50$, $f = 1.96$. Hence in the example of Fe, there is a $\sim 6\%$ deviation from a linear relationship if $M_0(T)$ decreases by 50%. In the case of Ni, we have $n \simeq 4.75$, $\Delta n \simeq 0.25$, and the deviation from linearity can be neglected. Generally, the smaller P_i the better the assumption that the measured polarization of the cascade P_C is proportional to the magnetization. In the following, we shall assume that $P_C(H, T)$ is proportional to $M(H, T)$.

A similar reasoning can be applied to P_{hv} observed in photoemission near photoelectric threshold. This is of experimental interest, as particularly laser-induced photoelectrons come in large quantities and allow time-resolved magnetometry. The difference is that the initial polarization P_i is no longer equal to the average polarization $\Delta n/n$ in the d band, but is equal to the combined polarization P_i and P_f of the initial and final state involved in the photoexcitation [3]. It is then clear that P_{hv} is enhanced as with cascade electrons. Because the enhancement $f \geqslant 1$, it cannot change the sign of the observed P_{hv}. This has the consequence that the number and sign of spectral features observed in spin-polarized photoemission is not changed in the transport of the electrons to the surface, but the amplitude and shape of the peaks might be altered depending on P_i and P_f. A more complete theoretical treatment based on the proposed simple model for de-excitation is of course highly desirable.

2. Ferromagnetism at surfaces of model materials

The most detailed information on magnetism at surfaces comes from photoemission (PES) and inverse photoemission (IPS). These techniques can determine the dispersion relation $E(k)$ of electronic states below and above the Fermi level. The energy states of majority and minority spin electrons are separated in the ferromagnetic state by the energy- and momentum-dependent exchange splitting. Spectral features result from optical transitions into bulk as well as into surface- or adsorbate-induced states. By analysing the spin polarization of the emitted electrons (in PES) or by observing the bremsstrahlung emitted when a spin-polarized electron beam strikes the surface (in IPS), the majority and minority bands in ferromagnets can be investigated separately.

One generation of researchers struggled to prepare the ground for what are today the most effective tools in metallic magnetism [4]. In PES, spin analysis by Mott detectors involves intensity reduction by four orders of magnitude which comes after the small photoemission currents obtained with monochromatic light sources and after the emitted electrons have been subject to energy and momentum selection. In IPS the quantum yield for production of bremsstrahlung is less efficient than the photoelectric excitation in PES by about $\alpha^2 = 10^{-4}$ where α is the fine-structure constant. IPS therefore required the development of powerful spin-polarized electron sources based on photoemission from GaAs photocathodes.

Most of the work in PES and IPS deals with the question of the temperature dependence of the exchange splitting ΔE_{ex} between spin-up and spin-down states. The experiments revealed a complex behaviour of ΔE_{ex} which seems to depend on T in some parts of the Brillouin zone, but not in others. This can be explained by considering the group velocity of the electron states. For low group velocity, the electrons are confined to one particular location where the local exchange field might be determined by atomic properties which do not depend on temperature. For high group velocity, the electrons experience the average exchange field which will be reduced at T_C.

Donath [21] points out that in all PES experiments on Ni, the only bands investigated so far have been those in which both the majority and the minority states are occupied. Yet fully occupied bands, even if spin split, do not contribute to the magnetization. The bands which generate the magnetization in Ni are the ones in which the majority bands are full, but the minority bands are partially occupied. The exchange splitting of these 3d bands is T-dependent and vanishes at T_C. To verify this with the experiments some reasonable assumptions concerning the position and width of the bands have to be made [21]. Then, the results obtained with the 3d bands of Ni are compatible with the basic assumption of band magnetism [22]:

$$\Delta E_{ex} = I_{eff} n_B(T) \tag{5}$$

with a temperature-independent effective exchange interaction I_{eff}, and $n_B(T)$ the Bohr magneton number per atom. However, one must expect that I_{eff} as well as $n_B(T)$ will be different at the surface. In PES and in IPS low-energy electrons of a few eV kinetic energy are employed, and therefore the magnetic properties of the surface layer are important despite the fact that one has tuned to emissions from the bulk 3d bands. This can be shown quite clearly by comparing the temperature dependence of the total number of Bohr magnetons/atom $n_B^*(T)$ observed for example along the ΓX direction in IPS on Ni(110) [21] to the T-dependence of the bulk magnetization. We have

$$n_B^*(T) = \int_{E_F}^{\infty} (D^{\uparrow}(E) - D^{\downarrow}(E))\,dE \tag{6}$$

where $D^{\uparrow}$ ($D^{\downarrow}$) is the density of states for spin-up (spin-down) electrons. Figure 2 shows that $n_B^*(T)$ decreases faster with increasing T compared to the bulk magnetization $M_0(T)/M_0(0)$. $n_B^*(T)$ is in fact very similar to $P_C(T)/P_C(0)$ observed for instance by Abraham and Hopster [23] with cascade electrons of 0–10 eV energy on the same surface of Ni. Hence one measures magnetic properties typical for the surface. It will be shown in the next section that this is due to the fact that the probability of finding a spin wave, that is a reduced magnetization, is higher at the surface than in the bulk. The probability density of spin waves depends also on the effective exchange interaction I_{eff} which in turn might be modified dramatically by surface structure and chemistry. Only future experiments with electrons of high kinetic energies $\geqslant$ 1000 eV will make it possible to test bulk magnetism in electron spectroscopy.

Additional surface magnetic properties arise from the various types of electronic states introduced by the surface. Two classes of surface states have been identified: namely the crystal-induced states of the Schottky type and the image potential surface states.

The surface band S_1 on Ni(110) around the $\overline{X}$ point about 6 eV above E_F shows an exchange splitting of 170 ± 30 meV [21]. This band is centred in the first layer of Ni, and its exchange splitting depends on chemisorption. As S_1 is not occupied, only indirect conclusions on primary magnetic properties are possible from these observations. Yet one old misconception on surface magnetism can be removed, namely that the surface is magnetically dead in clean Ni and/or that chemisorption of, e.g., O causes a dead layer. In older experiments, it was often concluded that chemisorption of O induces a magnetically dead layer, yet today it is clear that even

the O 2p bands are spin split, while the direct d-band emission from the substrate might be simply attenuated.

Image potential surface states are centred outside the surface. While there is experimental evidence that these states can also be exchange split, the splitting is certainly very small compared to the exchange splitting of the 3d and even the sp bands [24]. It results from the spin-dependent energy position of the gaps in the projected bulk band structure [25]. The small or vanishing exchange splitting of the image potential surface states explains the absence of spin polarization of thermo-emitted electrons observed with Fe and Ni by Vaterlaus, Milani, and Meier [26]. Helman and Baltensperger [27] point out that thermo-emitted electrons are extracted from the electron cloud trapped outside the surface by the image potential which is not at all or only very weakly spin polarized.

2.1. *Exchange interactions at the surface*

The exchange constant J is defined by the exchange energy $JS_i \cdot S_j$ between the magnetic moments S_i and S_j of atoms i and j in a solid. The exact meaning of J depends on the theoretical model. J cannot be reliably calculated from first principles nor can it be measured directly. However, J is related to T_C and directly linked to measurable quantities such as the spin-wave energy, the thickness of a domain wall, or the exchange splitting ΔE_{ex} in equation (5). It is expected that the exchange interaction J_S at the surface of a ferromagnet is different from the spherically averaged value of J in the bulk, and that this difference depends on the crystallography and the chemical composition of the surface. The altered J at the surface may lead to dramatic phenomena. For example, the surface may exhibit ordering at $T_{CS} > T_{CB}$, where T_{CB} is the Curie point of the bulk, or antiferromagnetic order might exist at the surface of a ferromagnet. Magnets traditionally provide the prototype examples for surface critical phenomena such as order–disorder transitions and unmixing in binary alloys, gas–liquid condensations in a fluid, and structural transitions, to name but a few [2]. Moreover, the surface is the source of the exchange field transferred across an interface to a second magnetic material or crystallite, so surface magnetism is the key to the exciting phenomena observed in magnetic multilayers that are of central interest in present day magnetic research. For these reasons, there is considerable interest in the direct experimental study of the surface exchange interaction J_S. Scholl *et al* [28] have shown that J_S can be determined in units of the bulk exchange J by measuring the temperature dependence of the local magnetization $M_S(T)$ at the surface. Dramatic increases or decreases of J_S/J can be obtained by depositing fractional layers of additional metal atoms on the surface. This observation opens a largely unexplored area for further basic investigations, and even suggests the possibility of magnetic interfaces designed to meet specific requirements.

2.1.1. $M_S(T)$ *in the spin-wave regime.* At low temperatures $T/T_C < 0.4$, the thermal decrease of the relative magnetization $M(T)/M(0)$ is caused by excitation of non-interacting spin waves. At the surface of the ferromagnet, the spin waves are reflected. Since the surface is a free end, the spin waves of any wavelength will exhibit an antinode in the last layer S. This leads to a characteristic profile of the local magnetization $M_{S-i}(T)/M_{S-i}(0)$, where $i = 0, 1, 2, \ldots$. The relative probability k_{S-i} of finding a spin wave in the layer $S - i$ compared to the probability in the bulk depends on the local exchange interaction J_S [29]. If J_S is equal to the average exchange interaction J in the bulk, $k_S = 2$ [30]. If, however, $J_S/J > 1 (< 1)$

the local density of spin waves in the surface decreases (increases) and the relative probability k_S of finding a spin wave in the surface compared to the probability in the bulk is $k_S < 2 (k_S > 2)$. The thermal decrease of the local magnetization $M_{S-i}(T)$ is related to the decrease of the relative bulk magnetization $M_B(T)$ by

$$(M_{S-i}(0) - M_{S-i}(T))/M_{S-i}(0) = k_{S-i}(M_B(0) - M_B(T))/M_B(0). \tag{7}$$

Using the surface Green's function technique, the density of spin-wave states and with it the local magnetization $M_{S-i}(T)$ can be calculated for each layer. It turns out that k_{S-i} is approximately independent of temperature, at least in the range $0.1 \leqslant J_S/J \leqslant 3$. The degree to which k_{S-i} is independent of temperature can also be experimentally verified by independent measurements of the bulk and surface magnetization.

Figure 3 shows the temperature dependence of the spin polarization P_C of the low-energy cascade electrons versus the temperature dependence of the bulk magnetization for the amorphous ferromagnet $FeNiB_{0.5}$ [31]. This material has a Curie point of $T_C \simeq 700$ K. It is particularly suited to testing the predictions [29] because the thermal decrease of the bulk magnetization is well described by spin-wave theory due to the near absence of magnetic anisotropy. Figure 3 shows that the predictions of equations (7) are met within the experimental limits of only $\pm 0.1\%$, even when the last layer is not clean, but modified by the deposition of half a monolayer of Ta. This modification changed the prefactors k_{S-i} considerably, namely from ~ 2 to ~ 5, yet the linear relationship is still preserved. *This documents a major progress in the understanding of $M_S(T)$ at low temperatures.*

For many ferromagnets, the thermally induced decrease of M_B at $T/T_C \leqslant 0.4$ is given by Bloch's law

$$(M_B(0) - M_B(T))/M_B(0) = CT^{3/2} \tag{8}$$

where C is a constant. With k_{S-i} independent of temperature, the thermal decrease of M_{S-i} follows the $T^{3/2}$ law according to equation (7) as well. Figure 4 shows the relative change of the magnetization $\Delta M_{S-i}(T)/M_{S-i}(0)$ calculated for a cubic crystal structure at constant temperature $T/T_C = 0.3$ for three cases in which the exchange interaction $J_{S\parallel}$ on a path within the surface layer as well as the exchange interaction J_S on a path perpendicular to the surface layer has been varied with respect to the average value of J in the bulk [28]. If $J_{S\parallel}/J = 1$ and $J_{S\perp}/J = 1$, that is, if the exchange is not different at the surface, the thermal decrease of the surface magnetization is twice that of the bulk. The weakening of the exchange on a path perpendicular to the surface enhances the thermal decrease of the surface magnetization, whereas the strengthening of the exchange parallel to the surface can make it even smaller than the thermal decrease of $M_B(T)$. For instance, if $J_{S\perp}/J = 0.1$ and $J_{S\parallel}/J = 1$, M_S decreases by as much as 20% at $T/T_C = 0.3$, whereas if $J_{S\perp}/J = 1$ and $J_{S\parallel}/J = 3$, M_S decreases by only 4%. In the latter case, the magnetization at the surface is actually higher than the bulk value. The calculations show that this condition is realized only when $J_{S\parallel}$ is strengthened, not by strengthening only $J_{S\perp}$.

An alternate cause of the thermal stabilization of the surface magnetization might be found in the surface anisotropies. Pini and Rettori [32] have studied the effect of a surface single-ion anisotropy on the surface magnetization, and find that a strong

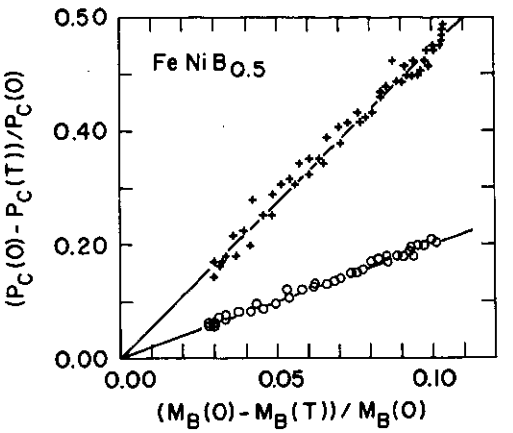

Figure 3. Temperature dependence $\Delta P_C(T)/P_C(0)$ of the cascade electron spin polarization versus the temperature dependence of the bulk magnetization $\Delta M_B(T)/M_B(0)$ for two differently prepared surfaces of $FeNiB_{0.5}$, according to [31]. The weak temperature dependence of P_C occurs with a surface as close to bulk composition as possible, whereas the strong T-dependence of P_C is obtained by deposition of half a monolayer of Ta.

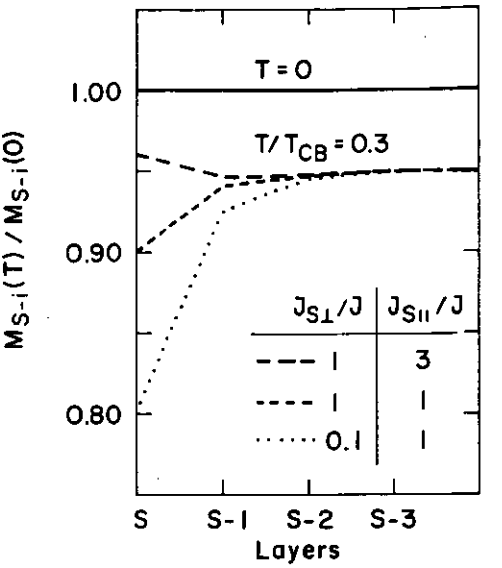

Figure 4. Calculated relative layer magnetization $M_{S-i}((T)/M_{S-i}(0))$ for the surface layer S and the subsequent layers $S - i$ with $i = 1, 2, 3$ and 4 is shown. The exchange J_S in the surface layer is modified on a path perpendicular ($\perp$) or parallel ($\parallel$) to the surface with respect to the spherically averaged value of J in the bulk. The calculation is for the FCC lattice of $Fe_{78}Ni_{22}$ at $T/T_{CB} = 0.3$, where $T_{CB} = 850$ K, from [28].

surface anisotropy can thermally stabilize $M_S(T)$. Bruno and Renard [33] estimate that the single-ion anisotropy of Fe for example might be as high as 1 meV/atom. However, even with this high anisotropy K, the ratio K/J is still as low as 0.06, far too little to explain the giant effects observed in the experiments. However, in the cases where J_S is sufficiently weak, surface anisotropies will have a dominant influence on $M_S(H, T)$ as will be shown in section 2.2.

2.1.2. Experiments for measurement of surface exchange. Figure 4 shows that the surface-induced modification of k_{s-i} extends only a few layers below the surface. Therefore, the probing depth of the magnetic measurement has to be of the order of the lattice parameter. Conversion-electron Mössbauer spectroscopy has the required monolayer resolution yet it is difficult to extract M_S from the measurement which takes a long time. At any rate, systematic studies of M_S in the spin-wave regime have only been performed so far by measuring the spin polarization P_C of the low-energy cascade electrons. The absolute value of P_C cannot be interpreted at present because it depends on the attenuation by scattering into the hole states of the d band as explained in 1.2. In the spin-wave regime, the assumption that P_C is proportional to some weighted average of $M_{S-i}(T)$ holds according to equation (4). The average can be estimated from the probability

$$P_{S-i} \times \text{constant} \times \int_{S-(i+1)}^{S-i} e^{-x/\lambda}\, dx \qquad (9)$$

that the electron originated in the layer $S-i$ at a distance x from the surface, where λ is the probing depth of cascade electrons displayed in figure 1. Equation (9) allows one to calculate k_{eff} which connects the observed P_C to the known bulk magnetization M_B:

$$\Delta P_C(T)/P_C(0) = k_{\text{eff}}\,\Delta M_B(T)/M_B(0). \tag{10}$$

The information on J_S/J is contained in the experimentally determined value of k_{eff}. For the ideal surface with bulk exchange at the surface $J_S/J = 1$, one obtained $k_{\text{eff}} = 2$, 1.5, 1.3 and 1; for $\lambda = 0$, 0.3 nm, 0.6 nm, and ∞ respectively. Uncertainty in the probing depth λ of ± 0.1 nm introduces an uncertainty in k_{eff} of $\pm 10\%$.

The substitutional $Ni_{78}Fe_{22}$ alloy (permalloy) with FCC crystal structure and a Curie point $T_{CB} = 850$ K is distinguished among the Fe–Ni alloys by its low magnetic anisotropy which makes it particularly suitable for this type of study. There is no general agreement on the proper theoretical description of the temperature dependence of M_S in permalloy [34]. For the sake of simplicity, and within an accuracy adequate for a first study, one assumes the simple Bloch law, equation (8). The constant, $C = 1.23 \times 10^{-5}$ (degree)$^{-3/2}$ was determined by a fit of the data for M_B obtained in a vibrating sample magnetometer to equation (8) in the temperature range $4\,\text{K} \leqslant T \leqslant 270$ K.

The films were sputter deposited by Xe ions from a plasma gun onto a Cu band 4 mm wide [28]. The Cu band was mounted on a UHV precision manipulator and could be brought to temperatures $90\,\text{K} \leqslant T \leqslant 450$ K. An electric current flowing through the Cu band provided a magnetic field $H \leqslant 2$ kA m^{-1} parallel to the surface of the band. First, a thick permalloy film with uniaxial anisotropy was deposited, exhibiting nearly square magnetization loops with coercivities < 0.5 kA m^{-1} as evidenced by *in situ* magneto-optic Kerr measurements. On top of the surface of the permalloy, other metals were deposited as desired. Film thicknesses were measured by a previously calibrated quartz microbalance. The chemical composition of the various surfaces was obtained by rotating the sample in front of a CMA Auger spectrometer. With each surface, a full cooling and warming cycle was performed, and the first and last points were measured at the same temperature. No irreversible changes occurred during the measurements.

With clean permalloy surface, $k_{\text{eff}} = 1.94$. Since we expect at most $k_{\text{eff}} = 1.5$ for $J_S = J$, this indicates that J_S is reduced from the bulk value in the surface of permalloy. This surface was the cleanest permalloy surface prepared, with C and O contaminants below $\sim 1\%$ of a monolayer each. The saturation cascade polarization was $P_0(T \to 0) \simeq 20\%$. The magnetization in units of the Bohr magneton per atom in $Ni_{78}Fe_{22}$ at $T \to 0$ is $\simeq 1.05\,\mu_B$/atom. The average number of electrons per atom is 9.56. Deducting 5% for the contribution of the orbital moment, the average spin polarization of the valence electrons is $P_i = 1.00/9.56 \simeq 10\%$. The enhancement of P_C over P_i has been observed with all ferromagnetic metals and is explained by equation (4). Clean permalloy surfaces are difficult to prepare. Fe segregation occurs readily upon mild annealing and upon oxygen adsorption [35], increasing $P_C(0)$. On the other hand permalloy surfaces passivated by exposure to air yield a lower cascade polarization of $P_C(0) \sim 10\%$. Consistent with the findings of [35] there is probably a protective coating of antiferromagnetic Fe^{3+} oxide, and the spin-polarized cascade electrons originate in the Ni-rich subsurface.

Deposition of 0.1 nm of Fe onto the clean permalloy surface corresponding to $\sim 60\%$ of a monolayer produces $k_{\text{eff}} = 0.51$, which means that the exchange in the

surface is strongly enhanced. This result can be reproduced by numerical calculation of k_{eff} with the assumption that the exchange is enhanced considerably in the first three surface layers, namely, if $J_{S\|}/J = J_{S\perp}/J = 3$, $J_{(S-1)\|}/J = J_{(S-1)\perp}/J = 3$, and $J_{(S-2)\|}/J = J_{(S-2)\perp}/J = 2$. Such a choice of the exchange parameters leads to the best fit to the observed $\Delta P(T)/P_C$ in the sense that the calculated weighted average of the surface magnetization obeys a very good $T^{3/2}$ law with $k_{\text{eff}} = 0.51$. It is not easy to determine the exchange parameters unambiguously but the following general considerations can be used to narrow down their range of variation considerably: (i) strengthening of $J_\perp$ alone cannot reduce k_{eff} below $k_{\text{eff}} = 1$. It follows that a large strengthening of $J_\|$ is required; (ii) strengthening of $J_{S\|}$ in the surface layer only can reproduce the magnitude of the observed effect with $J_{S\|}/J = 5$ but it leads to a systematic deviation from the $T^{3/2}$ law, which is not observed. A good $T^{3/2}$ law with k_{eff} as small as 0.51 can only be obtained if $J_\|$ and $J_\perp$ are comparable and the strengthening of the exchange is distributed over more than one layer. With these restrictions a quite reliable fit is possible. In particular, one can be certain that $J_{S\|}/J = 3$ is the lowest bound on the surface exchange enhancement.

One consequence of such a strong enhancement of the surface exchange is that the surface transition T_{CS} should occur at higher T compared to the bulk transition [2]. Mamaev *et al* have indeed found $T_{CS} > T_{CB}$ with single crystals of Ni_3Fe [36]. The enrichment of the Fe at the surface of Ni_3Fe necessary for the enhancement of the surface exchange could have occurred by spurious segregation of Fe [35].

Adding more Fe to the 0.1 nm of Fe overlayer reduces the exchange again. At a total coverage of 0.6 nm of Fe, $k_{\text{eff}} = 1.73$ is obtained indicating that J has now fallen below the value of the clean permalloy surface. The bulk magnetic properties of the FCC alloys of Fe and Ni show similar behaviour of the exchange constant. T_{CB} increases as the Fe content grows from 28% to 40%, but further increase of the Fe content induces a rapid fall of T_{CB} and a reduction of the magnetization in units of the Bohr magneton per atom [37]. This has been attributed to antiferromagnetic nearest-neighbour exchange for Fe in the FCC structure [37]. The example illustrates the rich information on magnetism that may now be gained from studying the exchange interaction at surfaces in the spin-wave regime.

2.1.3. $M_S(T)$ *near the Curie point.* Near the second-order magnetic phase transition, the correlation length ξ becomes very large. Thus, surface corrections are more important near the critical temperature T_{CB} of the bulk. Clearly, the local magnetization in the surface layer, M_S, will differ from the bulk magnetization M_B. To describe the surface properties, a magnetic field H_S can be introduced that acts on the surface spins only. On approaching T_{CB}, $M_B \propto (1 - T/T_{CB})^{\beta_B}$ and $M_S \propto (1 - T/T_{CB})\beta_S$, where β_B is the critical exponent with which M_B vanishes and β_S that of M_S. Just as in the spin-wave regime, the local quantity M_S is accessible to local probes only such as Mössbauer spectroscopy, and spin-polarized electron emission, capture and scattering. The change of the magnetic exchange interaction at the surface can now lead to rather dramatic phenomena, for example the surface may have an ordering temperature T_{CS} different from the one in the bulk. Furthermore, antiferromagnetic order might occur at the surface of ferromagnets. Other types of magnetic surface reconstructions are conceivable as well. Mean-field theory is not quantitatively accurate near the phase transition, but according to Binder [2] it can

nevertheless provide a qualitative understanding of the phenomena. In this approach, the magnetization changes exponentially on approaching the surface. The correlation length ξ determines the distance over which the distortion introduced by the surface heals out.

Normally, $M_S < M_B$. The transition from the disordered state to this state is called the 'ordinary' transition. Figure 4 shows that this applies to the surfaces in which $J_S/J \leqslant 1$. If the exchange in the surface is increased to a critical value, one has $M_S = M_B$. The transition from the disordered state is now called the 'special' transition. If J_S increases further, $M_S > M_B$. In that case M_S can exist at temperatures where $M_B = 0$, that is the surface has a critical temperature $T_{CS} > T_{CB}$. Transition from disorder to $M_S \neq 0$, $M_B = 0$ is the 'surface' transition. The second transition in which $M_B \neq 0$ occurs on further cooling is called the 'extraordinary' transition.

Obviously it would be best to do experiments on modified surfaces of the same ferromagnetic bulk material like the ones described in section 2.1.2 with $Ni_{78}Fe_{22}$ and Ni_3Fe. It is then possible to observe these transitions as the exchange J_S is modified. Other experiments are on clean surfaces, or more appropriately, on surfaces as clean as possible. Of course such state-of-the-art surfaces have unknown magnetic exchange interactions and magnetic anisotropies, and the results are sometimes difficult to interpret in detail.

The spin dependence A of the elastic scattering of electrons has often been used in the experiments. With single-crystalline surfaces, A arises from a complex superposition of the spin dependence of the atomic scattering and interference. Despite the finite probing depth of 1.5 layers in low-energy electron scattering, one can assume that A measures M_S only as the magnetic correlation length ξ diverges near T_C. Furthermore, A is an uneven function of M_S as it changes sign when M_S changes sign. Therefore $A(T) \propto M_S(T)$ must be a good approximation when M_S is small which is generally the case near T_C. Hence spin-polarized low-energy electron diffraction (SPLEED) is a good technique to determine the critical exponents.

Alvarado *et al* [38] studied clean Ni(100) and Ni(110). Specularly reflected electron beams were used only, but both kinetic energy E_K and angle of incidence θ of the electrons were varied. Within experimental uncertainty, and for $13 \leqslant E_K \leqslant 67$ eV and $\theta = 15°$ and $60°$, both surfaces showed a transition point $T_{CS} = T_{CB}$ and a critical exponent $\beta_S = -0.80 \pm 0.02$. The fact that the result does not depend on E_K and θ supports the notion that $A(T) \propto M_S(T)$. Effects of surface layer contraction and magnetostriction are estimated to be negligible. Hence it appears that both faces of Ni simply show the ordinary transition. The theoretical values of β_S are also around 0.8 for the Ising, XY, and Heisenberg models. For the bulk magnetization, $\beta_B = 0.38$ is observed in neutron scattering.

Taborelli *et al* investigated Fe(110) with low-energy cascade electrons [39], and found that this surface also exhibits an ordinary transition only. Gd turned out to be more interesting. Two independent experiments, namely electron capture spectroscopy (ECS) [40] and SPLEED [41], showed that T_{CS} is at least 15 K higher than $T_{CB} = 293$ K. Hence in this case, the exchange J_S must be sufficiently enhanced in the surface to induce a surface transition followed by an extraordinary transition. Farle and Baberschke [42] found a lowering of T_C by 20 K compared to T_{CB} for one monolayer of Gd(001) on W(110). This does not contradict the above finding as Gd on its own substrate can easily be (slightly!) different from Gd on W. Rau and Robert [40] found both critical exponents for the surface and the extraordinary transition to

be 1.00 ± 0.01 while the theoretical predictions are somewhat uncertain. Sanchez and Moran-Lopez [43] predict that for a finite range of enhanced J_S, the surface transition in Gd(001) could be a first-order phase transition. The latter prediction depends on whether an external magnetic field is applied or not. Weller and Alvarado [44] find that $T_{CS} > T_{CB}$ hinges on the presence of an external magnetic field during cooling and take this as an indication that the first-order surface transition might be a reality. It is reassuring that with a contaminated Gd(001) surface, the phenomenon vanishes and $T_{CS} = T_{CB}$, that is a contaminated surface shows only the ordinary transition. This is expected as J_S is generally reduced upon chemisorption. A surface transition 20 K higher than the bulk Néel temperature of 228 K has also been detected at the surface of polycrystalline Tb by Rau *et al* [45].

EuS is a model Heisenberg ferromagnet in the bulk with $T_{CB} = 16.7$ K. The localized magnetic moments are generated by the half-filled $4f^7$ shell, hence there is no orbital moment and no major anisotropy in the bulk. Dauth *et al* [46] measured the critical exponent with SPLEED on the EuS(111) surface of a sample grown epitaxially on Si(111) and found $T_{CB} = T_{CS}$ and $\beta_S = 0.72 + 0.03$. Hence, this material shows an ordinary transition only. The semi-infinite, isotropic Heisenberg model [47] predicts $\beta_S = 0.84 \pm 0.013$. A magnetic surface anisotropy could be responsible for this discrepancy between theory and observation [47].

Ni_3Fe single crystals have been studied by Mamaev *et al* [36] as already mentioned in section 2.1.2. Information on M_S was obtained from the spin asymmetry A in specular elastic scattering of spin-polarized electrons at $E = 32$ eV and 58 eV. T_{CS} turned out to be substantially higher, namely 1050 K, compared to $T_{CB} = 850$ K. This result is consistent with the measurements in the spin-wave regime which show that slight enrichment of Fe at the surface enhances J_S dramatically.

On the whole, the existing experiments on magnetism at surfaces close to the Curie point fit well into the frame set by the theory. Particularly interesting future experiments include the systematic variation of J_S, e.g. by adding magnetic and non-magnetic surface impurities.

2.2. *Surface-induced magnetic structures*

A magnetic sample can be uniformly magnetized in a direction determined by the direction of the crystalline anisotropy, or by the shape, tensile stress, or by an external field. However, at the surface or interface with another material the magnetization often deviates from the direction in the bulk. In this case, magnetic structures have been induced by the surface or interface. Such surface-induced magnetic structures (SMS) have a decisive effect on the interpretation of surface magnetic measurements. Important magnetic bulk properties like coercivity are also determined by SMS. The strength of the experimental coercive field is generally lower by orders of magnitude than expected from theory unless one assumes that rudimentary traces of domain walls exist somewhere in the material, e.g., at grain boundaries, interfaces or surfaces [48]. These embryonic domain walls only have to be further developed and torn free from the interface or surface to reverse the magnetization [49]. In this way, the reversed domains do not have to nucleate from the uniformly magnetized state. This considerably reduces the energy barrier for reversing the magnetization. SMS can play the role of the embryonic domain walls.

Technological interest in SMS comes from the limitations they impose on the density of information stored in magnetic media and from the noise they may induce in all kinds of magnetic sensors.

There are basically three different situations which lead to the appearance of SMS.

(i) SMS induced without change of the primary magnetic properties by the demagnetizing fields if the magnetization direction in the bulk has a component perpendicular to the surface or interface. Examples include the famous closure domains at the (001) surface of HCP Co [50] and the transformation of Bloch-type domain walls into Néel walls at the surface of soft magnetic materials [51].

(ii) SMS induced by surface segregation. The best example is FeTb, in which Tb segregates at the surface and becomes antiferromagnetic by oxidation. A very thin layer of Fe is left behind in the subsurface with the easy direction of magnetization given by the shape anisotropy. In the bulk of 'amorphous' FeTb the easy direction of magnetization is induced by the conditions of sample preparation. If the magnetization direction is perpendicular to the surface in the bulk, it will turn until it is in the plane of the surface under most conditions [52]. There are of course many more examples; it is in fact unlikely that no surface segregation occurs in alloys or complex oxides such as the ferrites.

(iii) SMS induced by the change of the primary magnetic properties at the surface. The oldest and first example is the model ferromagnet EuO, in which the surface does not reach magnetic saturation at 10 K in external magnetic fields as high as 2.5×10^6 A m^{-1} while the bulk is of course uniformly magnetized in the field direction [53]. By doping EuO with a trivalent non-magnetic metal such as La, the deviations of the surface magnetization are reduced. This indicates that it is the weakening of the magnetic exchange J_S at the surface which is mainly responsible for SMS at ultrahigh-vacuum-cleaved surfaces of clean EuO.

Experimentally, the measurement of the spin polarization P_C of low-energy cascade electrons or photoelectrons offers the best possibility to detect the SMS of type 2 and 3. In experiments with low lateral resolution, one has to measure the surface magnetization curve $M_S(H)$ of the last few atomic layers. If $M_S(H)$ is different from the bulk magnetization curve $M_B(H)$, SMS exist in the range of external fields H in which the differences occur. Typical surface hysteresis loops observed on a number of materials with the external field in the easy direction show rounded edges as the external field approaches the coercive field from $H = 0$ while the bulk loops are square, possibly with some wings extending to higher fields, due to bulk material imperfections [54]. The interpretation of the surface magnetization curves is not unique as both the surface anisotropy K_S and the exchange J_S can be responsible for the difference to $M_B(H)$. The magnitude of the spontaneous magnetization $M_S(T)$ can also contribute as the magnetostatic surface anisotropy density $M_S^2(T)/\mu_0$ is an important factor determining SMS.

In the simplest possible model, one assumes that only the first layer is different from the bulk. The first layer is coupled to the second by the exchange energy. $J_{S\perp} S_1 \cdot S_2 = dA_{1,2}$ where S_1 and S_2 are neighbouring magnetic moments in the first and second layer respectively, d is the interlayer distance, and $A_{1,2}$ the exchange stiffness on a path perpendicular to the surface. The magnetic properties in the subsequent layers are assumed to be bulklike.

The (100) surface of an Fe single crystal, remanently magnetized in the (010) easy direction parallel to the surface at first sight seems to be an unlikely candidate for SMS. Figure 5 shows that the existence of SMS at Fe(100) requires that the magnetization has a component perpendicular to the surface. This is possible only at the expense of the large magnetostatic energy density $M_{S\perp}^2(T)/\mu_0$. Nevertheless, it can be argued

that SMSS may exist even in this case [55]. The total energy per unit area of the surface δ has three terms: the energy of the tail of a domain wall extending into the bulk, the exchange coupling between surface layer and bulk, and the magnetic anisotropy energy of the surface which is the sum of the magnetostatic and the crystalline anisotropy. δ depends on ϑ and ψ which are defined in figure 5. When δ is minimum for $\vartheta = \psi = \pi/2$, there are no SMSS. If, however, the minimum occurs for ϑ more than 2° from $\pi/2$, this is taken by definition as SMS, notwithstanding the difficulty in observing experimentally such a small deviation of M_S. The reasons why SMSS are likely according to this definition are the following:

(i) The precondition for the occurrence of SMS is that the easy direction of M_S is perpendicular to the surface. This condition is probably met as one knows that Fe(100) ultrathin films have the magnetization mostly perpendicular to the plane of the films (section 3). This means that the surface anisotropy $K_S > M_S^2/\mu_0$ and $K_S > 33\ K_B$, where K_B is the crystalline anisotropy in the bulk. Gay and Richter [56] in fact calculated $K_S = 100\,K_B$ for one monolayer of Fe(100).

(ii) Taborelli *et al* [39] reported a strong thermal decrease of $M_S(T)$ in the (100) surface of Fe. This implies weakening of the exchange stiffness $A_{1,2}$ (section 2.1.2).

(iii) Because of the fast thermal decrease of $M_S(T)$, the magnetostatic energy density M_S^2/μ_0 opposing the formation of SMS is also reduced at $T > 0$.

The simple one-dimensional model [55] underestimates the likelihood of SMS because more complex structures than the one depicted in figure 5 could reduce the magnetostatic energy even further. For instance, SMS waves with the perpendicular component $M_{S\perp}$ pointing alternately into and out of the surface have a lower stray field. This is analogous to the domains occurring in ultrathin films with perpendicular magnetization (section 3.3). More theoretical work is certainly needed to discuss SMS.

Much better information than that obtained from hysteresis loops might be achieved with techniques that have a high lateral resolution. Scanning electron microscopy with polarization analysis (SEMPA) has been applied by a number of authors to image the distribution of the magnetization in the first few atomic layers at the surface [50]. A highly focused primary electron beam is scanned along the surface of the sample, thereby producing copious amounts of low-energy cascade electrons whose spin polarization P_C is proportional to M_S in the surface area from which the cascade electrons originated. Lateral resolutions of 20 nm have been realized in SEMPA. Scheinfein *et al* [51] and Oepen and Kirschner [57] obtained the magnetization profile across a domain wall at its intersection with the surface. In agreement with earlier work it was found that a Bloch wall does not terminate abruptly at the surface. This would generate a large magnetostatic energy density as the magnetization direction in the centre of the Bloch wall would have to point perpendicular to the surface. To avoid this, the magnetization turns over and lies in the surface in either one of the two directions perpendicular to the plane of the Bloch wall. The resulting Néel-like walls at the surface minimize the magnetostatic energy. The magnetization profiles across surface Néel walls are asymmetric. When two surface Néel walls with opposite asymmetry meet, there is an offset which is clearly seen in SEMPA. The observations can be explained with micromagnetic theory [51] without assuming any change of primary magnetic properties at the surface, that is they are SMS of type 1. From figure 5 it is clear that these SMS extend about the width of one magnetic domain wall into the bulk, which amounts to > 100 nm with soft magnetic materials. Hence, apart from the superior lateral resolution of SEMPA,

the much simpler magneto-optic Kerr effect with a probing depth 10–20 nm has also been successfully used to study this type of SMS [58].

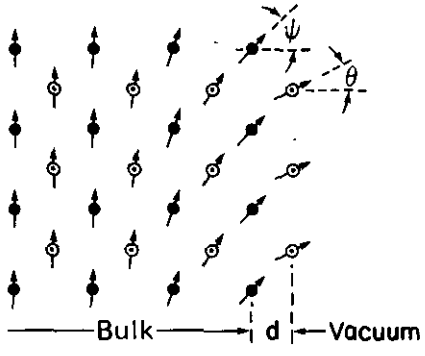

Figure 5. Model for a surface-induced magnetic structure (SMS) with the (100) surface of Fe as an example. The bulk is supposed to be remanently magnetized upwards with the surface anisotropy K_S perpendicular to the surface. It is assumed that only the first layer with lattice spacing d is different from the bulk. Atoms at circled positions are out of the plane of the drawing.

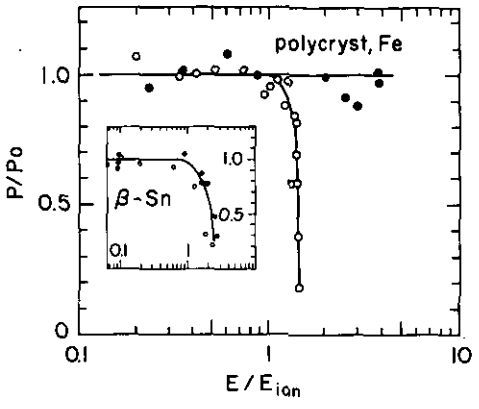

Figure 6. Relative photoelectron spin polarization P/P_0 of pulsed-laser-excited photoelectrons. P_0 is the polarization of photoelectrons emitted at very low light intensity. The open circles are for a long laser pulse (20 ns duration) and the filled circles for a short laser pulse (30 ps duration). The calibration of the laser pulses is in units of E_{ion} which is the energy at which positive ion emission sets in. $E = E_{ion}$ approximately indicates melting. With β-Sn, P is due to optical pumping with circularly polarized pulses, and there is no difference between short and long pulses. This proves that the equilibrium between the hot electrons and the phonons is established much faster than with magnons. From [61].

2.3. Surface magnetism off-equilibrium

When a magnetic field is applied suddenly to a magnetic material, the magnetization must change to reach a new equilibrium. This is a classical topic in magnetism, and the reversible and irreversible domain wall motions, Barkhausen jumps and processes of magnetization rotation have been studied for a long time. However, with the advent of intense pulsed laser beams, a more fundamental issue can be addressed as well. In the focus of such a laser beam, large amounts of energy may be deposited in a solid in an extremely short time. The energy is initially generated in the form of electron–hole pair excitations, that is the electron gas in the solid is heated in a few femtoseconds. The hot electron gas generates phonons. The establishment of the equilibrium temperature between the electron gas and the phonons takes about 10^{-12} s. In a magnetic solid, the electrons and to a lesser extent also the phonons may generate spin waves (magnons) as well. It will be shown that the establishment of the magnetic equilibrium temperature takes as long as 10^{-10} s, the bottleneck being the transfer of the angular momentum to the lattice. Laser-induced photoemission of electrons makes possible the measurement of the spin polarization of the electrons as

it changes while the thermal equilibrium is established in a magnetic solid. It should be noted that the spin polarization is the only property of the photoelectrons that is not affected by the heavy space charge generated in laser-induced photoemission. This is due to conservation of angular momentum in the space charge cloud [59]. Apart from its basic interest and novelty, this has also technological implications, for instance in thermomagnetic recording where the storage medium is heated by short laser pulses to induce magnetization reversal [60].

The fact that the photoelectrons probe only the surface has several important implications. In laser heating, there is the problem that the temperature is not homogeneous over the absorption depth of the light of $\sim$ 10–20 nm; yet as the low-energy photoelectrons from transition metals probe only $\sim$ 0.5 nm from the surface the temperature can be considered homogeneous over the depth of information. Generally, ultrafast magnetometry should become a key issue in surface magnetism. It will make it possible to perform surface magnetic measurements at higher temperatures which can normally not be done because of segregation by diffusion of atoms. As this diffusion is a slow process, fast heating at a rate of nanoseconds where electrons, phonons and magnons are in equilibrium combined with ultrafast measurement of the magnetization at the picosecond level will allow one to study delicate surfaces even at elevated temperatures.

Further, the establishment of the magnon equilibrium temperature can now directly be determined. It depends on the mechanism by which the electron spin is coupled to the lattice, that is on the magnetic anisotropy. In order to depolarize the electrons or to change the direction of the spin polarization in a solid, one needs to transfer angular momentum to the solid. Hence the measurement of the spin–lattice relaxation time provides basic information on the magnetic anisotropy which has its origin in the spin–orbit (l, s) interaction. With surfaces, the (l, s)-coupling can be very different from the bulk, because the crystal symmetry is broken and the orbital moment is quenched to a lesser extent than in the bulk.

Upper and lower limits for the time needed to establish thermal equilibrium of the magnetization in a solid have been obtained with a quite simple experiment [61]. The sample, a polycrystalline piece of Fe, is magnetically saturated in an external field. The pulse of a laser is focused onto the surface of Fe in UHV. The laser pulse has two functions: (i) it heats the sample; (ii) it induces the emission of photoelectrons from it. The power of the pulse can be large enough to melt the Fe. The melting is signalled by the onset of positive ion emission. The spin polarization P of the photoelectrons measures whether or not the Fe is still magnetized. Figure 6 shows that P is reduced to zero on melting the Fe with a pulse duration of 20 ns. If, however, the laser pulse is only 30 ps long, the spin polarization of Fe persists even in the liquid state. This clearly shows that the establishment of magnetic equilibrium takes longer than 30 ps but less than 20 ns. One can also show with this technique that the establishment of equilibrium between the heated electron gas and the phonons is much faster as follows. For this experiment, the laser pulse has to be circularly polarized. Circularly polarized light can induce the emission of spin-polarized electrons, for instance in β-Sn. The polarization occurs only in a crystal, not in a liquid. The inset in figure 6 shows that the polarization of the optically pumped photoelectrons from β-Sn is reduced to zero on melting even when the laser pulse is only $\sim 10^{-11}$ s long. This proves that the equilibrium between phonons and electrons is established much faster than equilibrium with the magnons.

In a more complete experiment, using a heating pulse with photon energy below

photoelectric threshold and a probing pulse with photon energy above photoelectric threshold, the time τ needed for establishment of the magnetization equilibrium can be determined explicitly. The probing pulse is focused into a smaller spot in the middle of the focus of the heating pulse so that the temperature can be considered homogeneous even laterally. Vaterlaus *et al* found for a Gd film on an Fe substrate $\tau = (1.0 \pm 0.8) \times 10^{-10}$ s [62]. This technique can be applied to all kinds of materials. Due to the surface sensitivity of photoemission it is particularly suited to studying the relaxation of the surface magnetization and of the magnetization in ultrathin films.

3. Magnetism in ultrathin films

Ferromagnetic films in the range of one to several monolayers exhibit special magnetic properties that have a great impact on the general understanding of magnetism as well as on applications. Since the pioneering work of Neugebauer [63] and Gradmann [64], it is clear that monolayer ferromagnetism exists. Theoretically, 2D ferromagnetism should not occur for isotropic nearest-neighbour exchange except in the Ising model [65]. The existence of monolayer ferromagnetism proves therefore that the interactions are generally not isotropic, and that anisotropies play a crucial role.

Blügel [66] points out that metallic magnetism in 2D is not *a priori* restricted to those elements which exhibit magnetism in 3D. Because of the reduced coordination number of nearest-neighbour atoms the d-band width in 2D is considerably smaller than in 3D and the magnetic instability should occur for a much wider variety of transition metal elements. Fu *et al* [67] have predicted, based on their band structure calculations, that a monolayer of V grown epitaxially on Ag(100) or Au(100) should be ferromagnetic, while V itself is not a magnetic element. Similar predictions have been made for monolayers of 4d elements (Tc, Ru, Rh, Pd) [68] and for 5d elements (Os, Ir) [66] on Ag(100). The magneto-optic Kerr effect [69], and spin-polarized photoemission and secondary electron emission are convenient and reliable probes to search for new ferromagnets, but to date have not confirmed any of these dramatic predictions. Only the electron capture experiment by Rau *et al* [70] confirmed ferromagnetism with 1 monolayer (ML) vanadium on Ag(001) at temperatures as high as 220 K. For 5 ML V on Ag(001), these authors even determined the critical exponent to be $\beta = 0.128 \pm 0.01$ in perfect agreement with the expectation of $\frac{1}{8}$ for a 2D Ising system. This is in striking contradiction to the results of spin-polarized photoemission by Stampanoni *et al* [7] who find no evidence of ferromagnetism in 1–3 ML V/Ag(001) down to 30 K and in external fields up to 1.5 MA m^{-1}.

In the case of Cr, the experiments demonstrate in unison that there is no ferromagnetism in ultrathin layers. Meanwhile calculations seem to show that antiferromagnetism is what one should expect for instance with Cr/Au(100) [72].

As the search for exotic 2D ferromagnets has not been successful so far, the experiments are done with ultrathin layers of Fe, Co, Ni and the 4f elements. Most of the work is with single-crystal epitaxial layers, but additional interesting aspects of 2D magnetism can also be studied with polycrystalline sputtered films as will be shown below.

Surprisingly, even the very simple measurements have proven to be difficult and often cannot be taken at face value, as for instance the determination of the thickness of the film.

Landskron *et al* [73] show in the case of Fe on Cu that an error of a factor 2 can easily be made in the number of monolayers if one uses break points of the Auger calibration curves for thickness determination. Kerkmann *et al* [74] determine the thickness of Co on Cu(100) by observing the quantum interference of low-energy spin-polarized electron waves reflected at the vacuum–substrate boundary of the ultrathin ferromagnetic film in optical analogy to interference at platelets. This should be the most accurate and most appropriate way to measure the thickness: it uses the ferromagnetic film thickness to generate a path difference for interference. Yet the result of the experiment appears to be in contrast to the findings of Schneider *et al* [75].

The precise determination of the thickness of the magnetic film is the prerequisite for answering the next simple question on the magnitude of the magnetic moment per atom in monolayer films at $T = 0$. *Ab initio* band calculations based on density functional theory now consistently predict enhancement of the magnetic moments in ultrathin films compared to the bulk value [76, 77]. Lugert and Bayreuther [78] have succeeded in measuring the magnetic moment of Fe(110) on Au(111) in a UHV–SQUID magnetometer. This measurement is the first and only one to confirm convincingly the trend of the theoretical predictions: the moment per atom increases as the number of layers is reduced and is 23% higher compared to the bulk value with 1 ML at $T \rightarrow 0$. It should be noted that the magnetometer responds to spin and orbital contributions. Hence the question on the Bohr magnetom number μ_B is still open.

The next important issue concerns the interdependence of magnetism and crystal structure. This is relevant particularly in the Fe/Cu(100) system where one expects that FCC Fe might be stabilized at room temperature. With the bulk, the stable phase at room temperature is BCC, but at $\sim$ 1000 K it is FCC. Extrapolation leads one to expect that the lattice parameter of FCC Fe at ambient T is 0.359 nm which is close to that of Cu with 0.361 nm. FCC Fe is interesting because various arguments seem to indicate that it could be non-magnetic or close to non-magnetic. Xhonneux and Courtens [79] find four different phases of Fe on Cu(001) as the number of monolayers deposited at room temperature increases: (i) from 1 to 3 ML a non-magnetic phase with 1×1 LEED pattern; (ii) from 3 to 5 ML a ferromagnetic phase with M perpendicular to the film plane and with a 5×1 LEED pattern; (iii) from 6 to 16 ML a non-magnetic phase with a 2×1 LEED pattern; and (iv) a pseudo-BCC phase, ferromagnetic, but M in plane for thicker films. Non-magnetic means here that no magnon–light scattering was observed at room temperature [79].

Non-magnetic Fe of several ML thickness was also previously detected in Mössbauer spectroscopy by Macedo and Keune [80], whereas most other authors did not observe it. The other experiments on Fe/Cu(001) include spin-polarized photoemission [81, 82], magneto-optic Kerr effect [83, 84], magnon-light scattering [85], ferromagnetic resonance [86] and high-resolution spin-polarized scanning electron microscopy [87].

With all these controversies, one should not lose sight of the exciting features observed with ultrathin ferromagnetic films: unexpectedly high transition points of up to 300 K even for 1 ML, spontaneous magnetization perpendicular to the plane of the film in many instances, oscillatory exchange coupling between two films separated by non-magnetic spacer layers over many atomic distances, and giant magnetoresistance. Careful measurements of the magnetization $M(H, T)$ provide the best sensor for the structure and quality of ultrathin films, and for the critical behaviour at the transition point.

3.1. Spontaneous magnetization in ultrathin films

The spontaneous magnetization $M_0(T)$ is defined as the magnetization generated by the quantum mechanical exchange interaction in the absence of an external magnetic field within one single Weiss domain. The temperature dependence of $M_0(T)$, particularly close to the magnetic transition point T_C provides a critical test of various concepts relating to phase transitions. The mean-field theory is surprisingly successful in describing $M_0(T)$. It yields a universal, that is, material-independent, temperature dependence of the reduced spontaneous magnetization $M_0(T^*)/M_0(0)$ with $T^* = T/T_C$. However, even in 3D, characteristic deviations from the mean-field curve occur close to the transition point $T^* \to 1$. These deviations are due to the fact that at $T^* = 1$, the magnetization does not break up into single independent paramagnetic atomic moments, but rather into clusters or blocks of spins which consist of many atoms having their magnetic moments still aligned parallel to each other. In 3D, the spin blocks have a diameter ζ and a lifetime τ given by

$$\zeta = \zeta_0 \epsilon^{-2/3} \qquad \tau = \tau_0 \epsilon^{-1/3} \tag{11}$$

where $\epsilon = 1 - T^*$. This means, that ζ and τ become very large as $T \to T_C$. For typical 3D magnets, one has $1000 > \zeta > 10$ nm and $10^{-10} > \tau > 10^{-11}$ s for $10^{-5} < \epsilon < 10^{-2}$. In bulk Fe for instance at 0.01 K from T_C one expects $\tau = 10^{-10}$ s and $\zeta = 1\mu$m. The spin blocks should thus directly be observable even with 3D bulk material in laser-induced spin-polarized photoemission (section 2.3). The occurrence of the fluctuations is common to all continuous phase transitions (phase transitions of second order) as there is no latent heat or volume work required when phase 1 transforms into phase 2. Hence there is no surface energy at the boundary between the two phases. The two phases can then transform into each other without supply of energy. If, by a thermal fluctuation, one phase is formed, it can grow at the expense of the other and *vice versa*. Therefore, close to T_C fluctuations between the two phases represent the thermally stable state of the system. However, laser-induced ultrafast magnetometry has also clearly demonstrated that the dominant bottleneck in the phase transition from the ferromagnetic to the paramagnetic state is the transfer of angular momentum to the crystal lattice. This must obstruct the fluctuations, and time scales as short as 10^{-11} s appear suspect in the light of the results reported in 2.3.

Already in the work of Weiss and Forrer in 1926 the fluctuations have manifested themselves although Weiss and Forrer did not recognize them as such. $M(H, T)$ of a homogenously magnetized Ni sphere looked like a paramagnetic Langevin function as T approached T_C. The Langevin function yields the z-component of the magnetization of a single ion aligned in an external field against thermal agitation. The problem with Ni close to T_C was that the magnetic moments appeared to be gigantic, that is they had to be built from the magnetic moments of thousands of atoms exchange coupled in the spin blocks. The volume V of the spin blocks can be estimated from $M(H, T)$ by equating the energy of the magnetic moment of the spin block in the applied field H to the thermal energy:

$$V = kT/\boldsymbol{M} \cdot \boldsymbol{H}. \tag{12}$$

This equation allows one to estimate the order of magnitude of the diameter $\zeta = V^{1/3}$ of the fluctuations.

In 2D, the fluctuations are expected to be larger and to extend over a larger interval of temperatures around T_C compared to 3D [88]. Conceptually, it is important to distinguish the fluctuations inherent in a continuous phase transition from superparamagnetic fluctuations. In 2D, crystalline defects, steps or roughness of the substrate can easily define a small island which is either not at all or only weakly exchange coupled to the rest of the ultrathin film. The magnetization direction of such islands can also fluctuate above a blocking temperature T_B. It will be shown below that the phenomenon of superparamagnetism is in fact the main obstacle in observing 2D magnetism.

It should be noted that different experimental techniques do not necessarily yield the same critical behaviour. This is of course described by the spin–spin correlation functions. It might be useful to discuss one simple and important aspect explicitly. Techniques employing Faraday and magneto-optic Kerr rotation, or electron spin polarization depend on the sign of $M_0(T)$. Averaged over a time and/or space much larger than ζ or τ given in equation (11), these techniques will yield zero at $T > T_C$ as the average magnetization direction of the spin blocks is zero. This is in contrast to other techniques which do not depend on the direction, but only on the magnitude of $M_0(T)$. These techniques include the spectroscopy of the hyperfine splitting and the exchange splitting ΔE_{ex} between spin-up and spin-down states. The splittings extend to $T > T_C$ in the time average as each spin block contributes independently of the direction of $M_0(T)$. How far above T_C the 'foot' extends depends on the range of neighbours generating the splitting. As an example, one sees that equation (5) can only be valid in the mean-field approximation.

3.1.1. The field dependence of the magnetization. Magnetization curves, that is the dependence of the magnetization M on the external field H, provide indispensable information on magnetic saturation and other primary magnetic properties such as the direction and strength of magnetic anisotropies. A variety of techniques have been adapted to measure the extremely small signals obtained from the magnetization of ultrathin films. Lugert and Bayreuther [78] for instance have used Josephson magnetometry to obtain accurate $M(H, T)$ curves. Bader [69] has shown that the magneto-optic Kerr effect can also have monolayer sensitivity. Spin-polarized electron beam techniques can be employed if the deleterious effects of the stray magnetic fields created outside the sample are avoided. The stray fields deflect the electrons due to the Lorentz force, and this may have intolerable effects on the location of the incident as well as the emerging electron beam and its focusing.

If H is applied perpendicular to the surface, electrons photoemitted from the film can be extracted parallel to the field lines [3]. The sample is located, for instance, in the bore of a superconducting coil. The light beam strikes the surface of the sample thereby causing the emission of photoelectrons. The electrons emerging near the axis of the coil can be extracted from the external magnetic field by suitable electrical acceleration parallel to the axis of the coil, and an electron beam can be formed for the measurement of P. Those electrons that emerge off-centre spiral away along the field lines and cannot be extracted. This configuration has the disadvantage that angle-resolved measurement of the electrons cannot be made and that energy analysis is difficult. However, it has the advantage that the sample may be exposed to very high magnetic fields; in fact spin polarization measurements have been performed up to $H = 5 \times 10^6$ A m^{-1} [3]. Figure 7 shows, as an example, the degree of the spin polarization versus the external magnetic field for 2.6 and 1 ML of Fe grown epitaxially

on Cu(001) measured at $T = 30$ K [81]. Fe on Cu(001) is a complex system, and controversial data have appeared in the literature. With the preparation conditions applied in [81], 1 ML exhibits no magnetic saturation, no remanence and no coercivity, while 2.6 ML clearly show the celebrated phenomenon of complete perpendicular magnetic remanence with a coercivity of $H_C \simeq 80$ kA m^{-1}. The question is: why does 1 ML not show perpendicular remanence? The uniaxial anisotropy K_S should appear at any surface whenever the cubic symmetry is broken, and the thinner the film, the larger the influence of K_S on the total anisotropy should be. The shape of $M(H)$ in the case of the 1 ML film and the absence of coercivity and remanence are the clear signature of superparamagnetism, that is the 1 ML film consists most likely of islands, either not at all or only weakly coupled to one another, for example at terrace ledges (steps) on the Cu substrate. $M(H, T)$ in fact allows one to estimate the anisotropy and the average diameter D of the superparamagnetic islands.

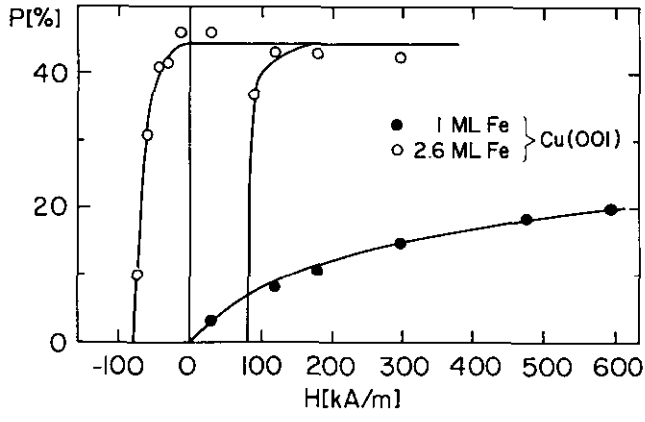

Figure 7. Spin polarization P along the magnetic field H applied perpendicular to the surface of epitaxial Fe on Cu(001). The photoelectrons are excited with photons of 5 eV from a xenon high-pressure arc, the temperature of the measurement is $T = 30$ K. From [81].

The physical idea behind this is the following: the magnetic anisotropy energy E of one island which is assumed not to interact with the others is given by

$$E = Ca_0D^2 \sin^2 \gamma \tag{13}$$

where $C = K_S - M^2/2\mu_0$, a_0 is the thickness of 1 ML and γ is the angle between the surface normal and magnetization M. E has minima at $\gamma = 0$ and $\gamma = \pi$ separated by an energy barrier Ca_0D^2. Thermal agitation may cause the magnetization to fluctuate between 0 and π. The time τ elapsed between two fluctuations has been calculated [89] to be

$$1/\tau = 10^9 \exp(-Ca_0D^2/2k_BT) \tag{14}$$

where k_B is the Boltzmann constant. As one measurement of P typically takes $\tau = 100$ s, one obtains from equation (5) the 'blocking' temperature $T_B = Ca_0D^2/(25.3k_B)$. For $T > T_B$, the observed remanence will be zero since M

fluctuates between $\gamma = 0$ and $\gamma = \pi$. With increasing H, the fluctuations are suppressed as $a_0 D^2 M \cdot H$ grows. Assuming that M is as in the bulk, and that C for 1 ML is the same as the one observed on 2.6 ML, namely $C = M \cdot H_C$, one obtains $T_B = 28$ K with an island size of $D = 10$ nm. $M(H)$ can be calculated from the Brillouin function in good agreement with the experiment. The above assumptions are reasonable and consistent with the experimental conditions. It is evident that $M(H)$-curves are essential for the understanding of magnetism. Looking only at the remanent magnetization as many researchers have done, one would have concluded that 1 ML Fe/Cu(100) is not magnetic at 30 K. In the interpretation of $M(H)$ based on superparamagnetism, the islands are fully magnetized up or down and localized on specific substrate sites. There is then no contradiction with the qualitative model of K_S due to Néel [90].

However, $M(H)$ cannot distinguish between superparamagnetism and the large fluctuating spin blocks inherent in the 2D Heisenberg model [88]. The spin blocks fluctuate at a fast rate and disappear and reform in arbitrary locations. This is in contrast to the superparamagnetic islands which are anchored to defects. Their magnetization direction fluctuates at a rather slow rate according to equation (14). Additional experiments are required to distinguish between inherent fluctuations and superparamagnetism.

If the external magnetic field is applied parallel to the sample surface, an awkward stray magnetic field is generated in front of the surface that can severely affect the emerging low-energy electrons. If the stray field is weak, in practice < 1 kA m^{-1} extending ~ 1 mm from the sample surface, low-energy cascade electrons emerging from the sample can still be focused adequately onto the entrance slit of the Mott polarimeter for measurement of P_C [91]. It is, however, clear that only soft magnetic samples can be saturated in weak external fields. $Ni_{78}Fe_{22}$ (permalloy) is an example of a soft magnetic material, but the question is whether the near compensation of crystalline anisotropy and magnetostriction will also occur with a few atomic layers and a further question is whether a *polycrystalline* material will exhibit a 2D transition. Mauri *et al* [91] prepared ultrathin permalloy films by sputtering a $Ni_{80}Fe_{20}$ target with a low-energy beam of Xe ions. The substrate consisted of a mechanically polished Cu band through which an electric current could be passed to produce a homogeneous magnetic field H at the surface. A film of about 50 nm of Ta was deposited onto the Cu band. Empirically, it turns out that soft magnetic permalloy can be obtained on this substrate surface even if the thickness is as thin as 0.45 nm, that is with nominally 2.5 layers of permalloy.

Figure 8 shows the dependence of the low-energy cascade polarization P_C on the external field H at various temperatures of the 0.45 nm thick $Ni_{78}Fe_{22}$ sample. At $T = 300$ K, the sample shows no measurable response to H, but at 289 K there is a linear $M(H)$ curve, indicating a giant enhancement of the susceptibility. The susceptibility increases up to 266 K, where effects of magnetic saturation start to be visible. At $T < 250$ K, remanence and coercivity appear within a few degrees, yet magnetic saturation is still higher than the remanent magnetization. From $T < 210$ K on, one obtains the square loops typical for a material with a uniaxial anisotropy magnetized in the easy direction of magnetization. Figure 8 shows qualitatively the same features as observed already by Weiss and Forrer in 1926 with a homogeneously magnetized Ni sphere at $T = T_C = 638$ K, yet the curved $M(H)$-dependences were limited to a smaller temperature interval $\epsilon = 1 - T^*$, and the applied fields were about 1000 times stronger. Hence the 2D phase transition is distinguished by a

larger diameter ζ of the spin blocks estimated from equation (12) and by a larger temperature interval ϵ in which critical phenomena are dominant, in agreement with the theoretical concepts [88]. However, positive proof that we are not looking at the unblocking of superparamagnetic islands in figure 8 cannot be derived from $M(H, T)$ curves alone.

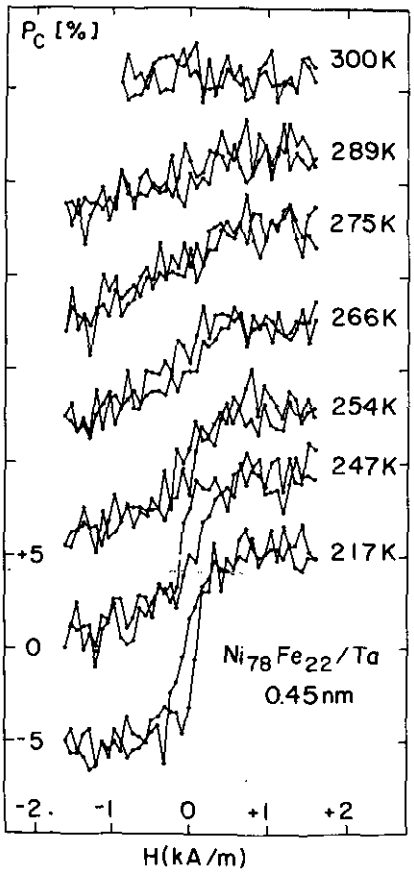

Figure 8. Field dependence of the spin polarization P_C of low-energy cascade electrons with a nominally 0.45 nm thick (2.5 ML) film of sputtered $Ni_{78}Fe_{22}$ on a Ta substrate at various temperatures. The large temperature interval of the enhanced susceptibility and the sudden appearance of hysteresis are evident. Data from [91].

3.1.2. The temperature dependence of the magnetization. The temperature dependence $M_0(T)$ of the spontaneous magnetization is what one needs to determine in the experiments. Figure 8 shows that it is difficult to obtain $M_0(T)$ from the observed $M(H, T)$. It involves extrapolation of $M(H, T)$ to $H = 0$ at $T =$ constant. This extrapolation is feasible at low T where magnetic saturation is clearly defined. Yet as T_C is approached, the extrapolation depends on preconceived ideas about how $M(H, T)$ should vary with H. The resulting uncertainty in $M_0(T)$ translates into a large uncertainty with which the critical exponent β and T_C can be determined. Close to T_C, scaling theory postulates

$$M(T^*)/M(0) = \epsilon^{\beta}. \tag{15}$$

Existing determinations of β and T_c have suffered from the uncertainty with which $M_0(T^*)$ could be determined or are questionable because the magnetization in an

applied field or the magnetic remanence was plotted instead of $M_0(T^*)$ [81, 92, 93]. Figure 8 demonstrates that the remanence can disappear faster than the polarization at $H = 0$ determined by extrapolation of the saturation, compare $M(H, 217)$.

Generally, the remanence is not equal to the spontaneous magnetization. Figure 9 shows the spontaneous spin polarization P_0 of the cascade electrons obtained by extrapolation of $P_C(H, T)$ to $H = 0$ for the 0.45 nm thick permalloy film of figure 8. At $T \ll T_C$, the remanent and the extrapolated polarization are identical as expected for a uniaxial material magnetized in the easy direction, and $M_0(T)/M_0(0)$ is readily obtained from the experiment. However, with the uncertainties existing in the extended critical region, it is clear that a variety of theoretical models for $M_0(T^*)/M_0(0)$ can approximately describe the measurements, depending on the range of temperatures considered and on the method of extrapolation. The Brillouin function for spin-$\frac{1}{2}$, which is the mean-field theory, is as good as any other model if one excludes the critical region. In the mean-field theory, $\beta = \frac{1}{2}$, but plotting for instance the remanent magnetization yields a steeper drop on approaching T_C, hence a smaller β.

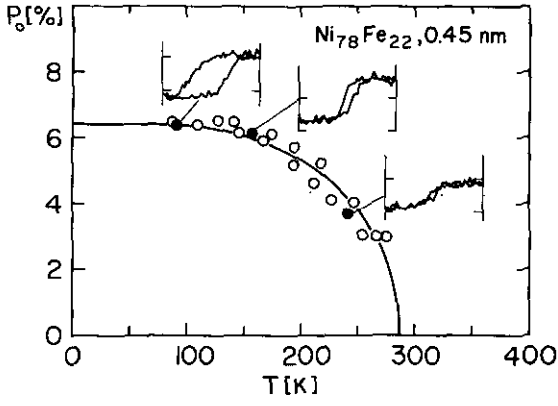

Figure 9. Spin polarization $P_0(T)$ obtained by extrapolation of $P_C(H, T)$ to $H \to 0$ for the 0.45 nm thick $Ni_{78}Fe_{22}$ sample of figure 8. The full curve is the Brillouin function for spin $\frac{1}{2}$. In the hysteresis loops shown at $T = 91$, 157 and 241 K, the difference between adjacent marks on the ordinate indicates 10% change of P_C while $-2 \leqslant H \leqslant 2$ kA m^{-1}. Data from [91].

The coincidence of $M_0(T)/M_0(0)$ with the predictions of mean-field theory at $T \ll T_C$ is in contrast to conventional spin-wave theory for 2D ferromagnetic films which predicts a rapid linear decrease at low T with low anisotropy materials such as permalloy [94]. Pini *et al* suggest that interaction of spin waves, which is more important in 2D than in 3D, can account for this failure [95]. Lugert and Bayreuther [78] and Mauri *et al* [91] note that earlier experiments in which a linear decrease of $M_0(T)$ at low T was frequently observed, are most likely explained by superparamagnetism in islands with a wide size distribution.

One unique feature of measuring the cascade electron polarization is that one can also study magnetic ultrathin films which are coupled to the 3D bulk through a non-magnetic interfacial spacer layer. Assuming that the exchange coupling through this interfacial spacial layer is sufficiently strong, the long-wavelength spin waves of the bulk material can pass through the exchange link as long as their wavelength is large compared to the microstructure and thickness of the region with the weakened exchange interaction. Then, the ultrathin film coupled to the bulk is connected to a reservoir of low-energy magnetic excitations. However, in an uncoupled 2D film, the low-energy magnetic excitations necessarily have to be quenched or it would not

be ferromagnetic. This is exactly what is observed. Figure 10 shows the temperature dependence of the magnetization of a 0.50 nm thick $Ni_{78}Fe_{22}$ film coupled to the bulk over 0.3 nm Ta, and $M(T)/M(0)$ for the isolated 0.45 thick film of figure 9. We see indeed that the magnetization of the coupled film decreases much faster with T than that of the isolated film. This demonstrates that the long-wavelength magnons are quenched in 2D films at low temperatures. How this quenching occurs is not clear at present. The magnetic anisotropy of the order of 1 kA m^{-1} is certainly not strong enough to explain it [96]. The question of why ultrathin films have such high transition temperatures still awaits a theoretical explanation.

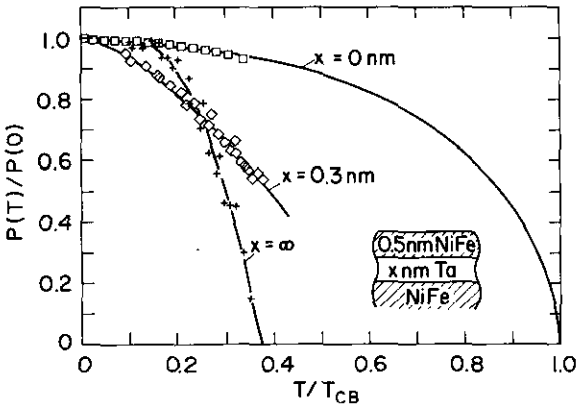

Figure 10. Comparison of the temperature dependence of the relative saturation spin polarization $P(T)/P(0)$ of cascade electrons between the isolated Ni–Fe film of figure 9 and a similar Ni–Fe film coupled over a 'weak' exchange link to the bulk of Ni–Fe. The T-dependence of the bulk magnetization is also shown (full line) with data obtained in a vibrating sample magnetometer. T_{CB} = 850 K is the Curie point of bulk $Ni_{78}Fe_{22}$. Data from [96, 91].

We now return to the problem of how to distinguish the unblocking of superparamagnetic islands from the breaking of the magnetization into fluctuating spin blocks. In the first case, the observed phase transition at T_0 would have to be identified with the blocking temperature T_B, equation (14), and not with the transition temperature T_C. With superparamagnetic islands, T_0 should depend strongly on the concentration of impurities and the quality of the substrate, as T_B must depend critically on defects defining the size of the island. The experiments confirm that T_0 does indeed depend strongly on impurities and the substrate preparation technique and even its temperature during deposition of the films [91, 97]. Hence in many cases one would tend to identify the observed T_0 with T_B. Note that for a sharp well-defined transition at T_B the islands must have a narrow size distribution which is possible but not normally the case. However, theory gives no hint as to how the true T_C should depend on the experimental conditions. Therefore, time- or spacially resolved experiments are necessary to decide whether the observed T_0 is T_B or T_C.

Kerkmann *et al* have addressed this question in an experiment with 1 ML of Co on Cu(100) [98]. The low-energy cascade polarization P_C from a spot as small as ~ 20 nm in diameter was measured in the absence on an external field. *The high lateral resolution makes it possible to measure directly the spontaneous magnetization*

$M_0(T)$ *within one domain without applying an external field.* Figure 11 shows that $|M_0(T)|$ decays fast with T defining a sharp transition temperature T_0. To decide between $T_0 = T_C$ or $T_0 = T_B$ one uses the fact that superparamagnetic islands are anchored to the location of the defects and that their magnetization fluctuates slowly according to equation (14). The radius R of the islands or the inherent spin blocks is given by T_0 and can be estimated from equation (12). With 1 ML Co, $d \simeq 0.2 \times 10^{-9}$ m, $T_0 \simeq 300$ K, $M_0 \simeq 1.7$ T, and the large response to an external field of $H = 8$ kA m^{-1}, one obtains $R \simeq 20$ nm. That is, the expected size of the islands is of the same order as the lateral resolution of the magnetization measurement. The time needed for accurate measurement of P_C is 10–100 s. As the islands unlock their magnetization direction at T_B, fluctuations should become observable. No such phenomena were seen within 1 K from T_0. Therefore, one can conclude that at $T = T_C$, the inherent phase transition with fast fluctuations occurred. In agreement with the general theory of 2D ferromagnetism, it is the large spin blocks that generate the phenomenal response to external fields in the critical region shown in figure 11.

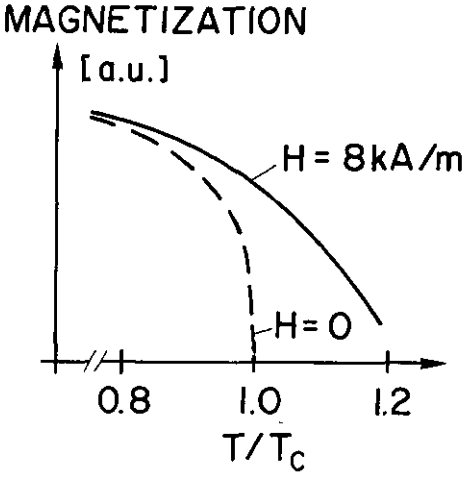

Figure 11. In-plane magnetization of one layer of Co on Cu(100) within one Weiss domain in zero applied field, measured via the low-energy cascade spin polarization with a lateral resolution of 20 nm, from Kerkmann *et al* [98]. The temperature dependence of the magnetization in an applied field of 8 kA m^{-1} is also shown.

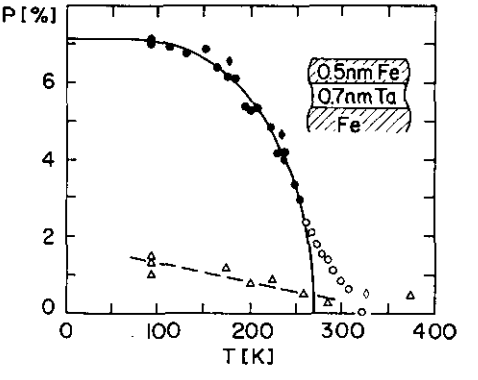

Figure 12. $P_C(T)$ of the low-energy cascade electrons of a polycrystalline Fe film 0.5 nm thick coupled to the bulk over a 0.7 nm thick Ta spacer. Triangles are observed immediately after deposition and after heating to 450 K, circles and diamonds after submonolayer contamination with C and O. The solid line is the Brillouin function for spin $\frac{1}{2}$ at $H_{ex} = 0$ fitted to the filled symbols. Data from [103].

An interesting temperature dependence of the remanent magnetization $M_R(T)$ has been observed with 3–5 ML FCC Fe on Cu(001). The Fe layers exhibit a 5×1 superstructure and are ferromagnetic with the easy direction of M_0 perpendicular at low T but parallel to the layers at high T [79, 81]. At the temperature T_S where M_0 switches from out-of-plane to in-plane, there is the possibility that the shape anisotropy is exactly compensated by the uniaxial crystal anisotropy. Hence at $T = T_S$ these films could be isotropic. With isotropic 2D ferromagnets one expects that $T_C = 0$ [65]—compare equation (18) to be discussed in section 3.2. Pappas *et al* [82] measured the T-dependence of the remanence $M_R(T)$ by observing the spin

polarization $P_C(T)$ of the cascade electrons. They found $|M_R(T)| = 0$ at $T \simeq T_S$, but apart from this indentation at T_S, $|M_R(T)|$ had the usual shape similar to the one of figure 11 at $H = 0$. This could mean that the system loses long-range order at T_S because it is isotropic. However, it is more likely that a domain structure reducing $M_R(T)$ to zero appeared at T_S. The lateral resolution in the experiment [82] was not sufficient to resolve the domain structure so the existence of the domains cannot be proven.

There are several reasons why the observation of a switching of M_0 from perpendicular to in-plane does not necessarily mean that one has an isotropic system. If one includes the higher-order term K_2 in the crystalline anisotropy besides the first order term K_1, the total anisotropy energy including shape anisotropy is

$$E = \tfrac{1}{2}\mu_0 M_0^2(T)\cos^2\vartheta + K_1\sin^2\vartheta + K_2\sin^4\vartheta \tag{16}$$

where ϑ is the angle between the surface normal and the magnetization. It is clear that even when $\frac{1}{2}\mu_0 M_0^2(T) = K_1$, there is still K_2 which is the reason why M_0 shows a continuous transition from perpendicular to in-plane [99]. Hence the system is never isotropic. Furthermore, Pescia and Pokrovsky [100] show that even when there is only a uniaxial anisotropy K_1, and even when $K_1 > \frac{1}{2}\mu_0(M_0^2 T)$ at all T, the magnetization may switch from perpendicular to in-plane at $T_S < T_C$. The anisotropic part of the free energy contains the entropy, and the entropy is larger with M_0 in-plane because all directions in-plane are possible. This, together with the strong fluctuations of the 2D Heisenberg model can explain switching of M_0 from perpendicular to in-plane. Hence the conjecture [82] of a re-entering spontaneous magnetization in Fe/Cu(001) as an explanation for the indented $M_R(T)$ is not compelling.

3.2. *Quasi-2D ferromagnetism*

Considering the large response of 2D ferromagnets to external fields, it is of considerable interest to study particularly the paramagnetic region $T > T_C$ in all kinds of external disturbances. So far, the closest realization of such 'quasi-2D' ferromagnets have been layered structures with small interplane coupling [101]. K_2CuF_4, for instance, crystallizes in magnetic layers with spin-$\frac{1}{2}$ and the dominant interaction is Heisenberg-like. The magnetic layers are separated by non-magnetic spacers. The relative perpendicular exchange coupling $J_\perp/J$ is of the order of 10^{-3}, with J the average exchange within the layer. A larger spin asymmetry of approximately 1% exists in the coupling within the layers. Due to this asymmetry, the easy direction of the magnetization lies in the plane of the layers, yet no direction in that plane is preferred. This situation corresponds to the XY-model in a certain range of temperatures near T_C. Spontaneous magnetization does not appear in the XY-model, but rather infinite magnetic susceptibility. Hence any small external field or magnetic anisotropy in the plane of the film will produce a substantial magnetization. The Kosterlitz–Thouless transition point is expected to shift to higher temperatures as the fields or the anisotropies in the plane of the 2D film increase [102].

Ultrathin magnetic films coupled through non-magnetic spacer layers to a 3D bulk ferromagnet make possible the engineering of quasi 2D ferromagnets as will be shown below. The magnetization of the overlayer film can be measured separately from that of the bulk ferromagnet by virtue of the small probing depth of the spin-polarized electron beam techniques.

Donath *et al* [103] studied 2D polycrystalline Fe films that were exchange coupled through nominally non-magnetic Ta layers of various thicknesses to bulk Fe. The exchange field H_{ex} transferred from the bulk through the Ta spacer layer into the overlayer film is the analogue of an external magnetic field applied parallel to the magnetic planes of the crystal. As long as one stays away from the Curie point of the bulk substrate, H_{ex} is constant in a small interval of temperatures. One magnetic layer in K_2CuF_4 corresponds to the ultrathin polycrystalline Fe film. This film is made up of many small crystallites which each have one or several easy directions of magnetization, but these directions are different in each crystallite if preferred crystallization directions and in-plane stress are absent. If the magnetic coupling between the crystallites is stronger than the individual anisotropies, their random orientation means that there is no preferred magnetization direction in the plane of the polycrystalline films just as with K_2CuFe_4. Furthermore, the preferential direction of M is in the plane of the Fe film rather than perpendicular to it because of the shape anisotropy. The ratio of the shape to the exchange energy is just about 1% in Fe. Therefore, the analogy to K_2CuF_4 is quite complete.

Hirakawa and Ubukoshi [104] have measured $H(H_{ex}, T)$ with K_2CuF_4 where H_{ex} was applied parallel to the layers. The explanation in terms of the XY model [102] is convincing, in particular the shape of $M(H_{ex} = \text{constant}, T)$ and the increase of the ordering temperature T_C with increasing H_{ex}. Although the magnetic transition is increasingly smeared out as H_{ex} increases, T_C is still clearly defined for instance by the point of inflection of the $M(H_{ex} = \text{constant}, T)$-curve.

It is clear from the experiments described in this chapter that superparamagnetism is the real obstacle in observing 2D magnetism, yet the magnetic properties are also the best sensor of superparamagnetic behaviour. This is illustrated in figure 12 where the spin polarization P_C of the low-energy cascade electrons from a sputter-deposited Fe film of 0.5 nm average thickness is plotted versus the temperature. The film is deposited onto a Ta spacer of 0.7 nm thickness which in turn sits on a substrate assembly consisting of a thin Fe overlayer on a thicker permalloy substrate layer. The Fe substrate overlayer is magnetically saturated in the direction of the measurement of P_C by exchange coupling to the permalloy film. In this way, the bulk substrate has the electronic properties of Fe near the substrate surface, but also the desirable soft magnetic properties of permalloy. This experimental approach allows one to saturate the Fe substrate magnetically in weak external fields, but has no other critical importance.

The 0.5 nm thick polycrystalline Fe overlayer film is now a quasi-2D film because a large H_{ex} is transferred into it from the substrate through the Ta spacer. Figure 12 shows that P_C is nevertheless very low rising to only 1–2% as the sample is cooled to $T = 100$ K. This polarization did not change on annealing to $T = 450$ K. However, with submonolayer contamination of C and O, P_C increased dramatically. The increase occurred despite the well-known fact that C and O attenuate the emission of spin-polarized electrons from the 3d band of Fe. Further adsorption of C and O did not affect $P_C(T)$ any more until severe contamination levels of the order of one monolayer or more were reached.

The key to the understanding of this phenomenon is that the shape of $P(H_{ex}, T)$ also changed dramatically, namely from more or less linear to a curve expected for $M(H_{ex}, T)$. The curve fitted to the filled data points in figure 12 taken with the submonolayer-contaminated film is the mean-field curve for spin $\frac{1}{2}$ in $H_{ex} = 0$. We see that this curve does represent the data well except close to the transition

point T_C where a tail occurs. This is due to the presence of H_{ex} transferred from the substrate and demonstrates that we now are dealing with a quasi-2D phase transition. The changes of P_C occurring during the conversion from the freshly deposited to the aged film are induced by the transition from superparamagnetism to ferromagnetism. In line with the findings of Egelhoff and Steigerwald [105], small amounts of contaminations such as C and O must have acted as surfactants allowing the Fe to lower its surface energy in order to spread out and gain the surface energy of uncovered Ta. This is in agreement with the observation that annealing does not induce the transition from superparamagnetism to ferromagnetism and that T_C as far as one can tell does not change in that transition. Hence figure 12 demonstrates that it is possible, with the help of minute amounts of contamination of C and O acting as surfactants, to avoid the obstacle of superparamagnetism and sputter deposit ultrathin polycrystalline Fe films on a Ta substrate in a stable ferromagnetic state.

The next step is now to prepare the 2D Fe films on a thinner Ta substrate in order to increase H_{ex} transferred from the substrate. It turns out that the changes in $P(H_{ex}, T)$ occurring with the adsorption of residual gas molecules are less dramatic with a thinner Ta spacer, that is, with increased H_{ex}. This is in agreement with the expectation that as H_{ex} increases, the superparamagnetic fluctuations must be increasingly suppressed. Finally, a stable $P(H_{ex}, T)$ is reached in all cases which again is well represented by the Brillouin function for spin $\frac{1}{2}$ at low T/T_C, but close to T_C a tail occurs which increases with decreasing thickness of the Ta spacer, that is, with increasing H_{ex}, consistent with the expectation for a phase transition in a quasi-2D system.

As the thickness x of the non-magnetic Ta spacer decreases, the Fe overlayer couples more strongly to the 3D magnetic substrate and crossover from 2D magnetism to 3D magnetism occurs. Figure 13 summarizes the results with Ta spacer thicknesses of $x = 0.3$, 0.5, and 0.7 nm thickness. The temperature is in reduced units $T' = T/T_{CB}$ where $T_{CB} = 1043$ K is the Curie point of bulk Fe; the T-dependence of the magnetization in bulk Fe is also given for comparison. The relative spin polarization $P(H_{ex}, T)/P(H_{ex}, 0)$ for the quasi-2D films is plotted in the stable ferromagnetic state. The transition points T_C are increasingly smeared out as H_{ex} grows, yet T_C is still clearly defined. The solid lines are calculated mean-field curves in an external magnetic field H_{ex}. They are not based on any theoretical model for quasi-2D films, yet they fit the experimental data well within the experimental uncertainty. From these fits one obtains $T_C = 421$, 344, 270 K, $H_{ex} = 32$, 16, 8 MA m^{-1} for Ta spacer thicknesses of $x = 0.3$, 0.5, 0.7 nm respectively. One sees that the *ansatz*

$$H_{ex} = H_0 e^{-\alpha x} \tag{17}$$

describes the dependence of H_{ex} transferred through the Ta spacer of thickness x taking $H_0 = 80$ MA m^{-1} and $\alpha = 3.1$ nm^{-1}. This value of H_0 corresponds to the molecular field in bulk Fe reduced by $\sim 30\%$ to take into account the smaller number of nearest neighbours in the surface.

Theoretically, both a space anisotropy and a spin anisotropy lead to an increase of T_C in quasi-2D systems. In fact, the *dependence of T_C on the anisotropies is the typical signature of the 2D system* as it does not occur in the 3D one. Noting that H_{ex} = constant in a temperature interval close to T_C of the overlayer, one is led to suppose that the observed shift of T_C is due to spin anisotropies yielding

$$T_C = C_1 T_{CB} / \ln(C_2 T_{CB} / H_{ex}) \tag{18}$$

where C_1 and C_2 are constants and H_{ex} describes the strength of the anisotropy [102]. This general form of the dependence of T_C on anisotropies is found with many different 2D models and assumptions. Combining equations (17) and (18) yields

$$T_{CB}/T_C = Ax + B. \tag{19}$$

The experimental data are consistent with equation (19) as shown in [103].

Figures 13 and 10 demonstrate that the transition from a magnetically isolated 2D film to a magnetic film coupled to the surface of a 3D ferromagnet is different in Fe and $Ni_{78}Fe_{22}$. The NiFe film is already part of the surface of the 3D substrate at the same thickness of the Ta spacer layer, where Fe is still clearly quasi-2D. This may be explained by the fact that NiFe has a very low intrinsic anisotropy compared to Fe. Furthermore, polycrystalline Fe in the present form seems to require substantial exchange fields transferred from the substrate to exhibit magnetic order which agrees with equation (18), whereas the origin of the high T_C in ultrathin NiFe cannot be explained by the magnetic anisotropy, which is low in this case.

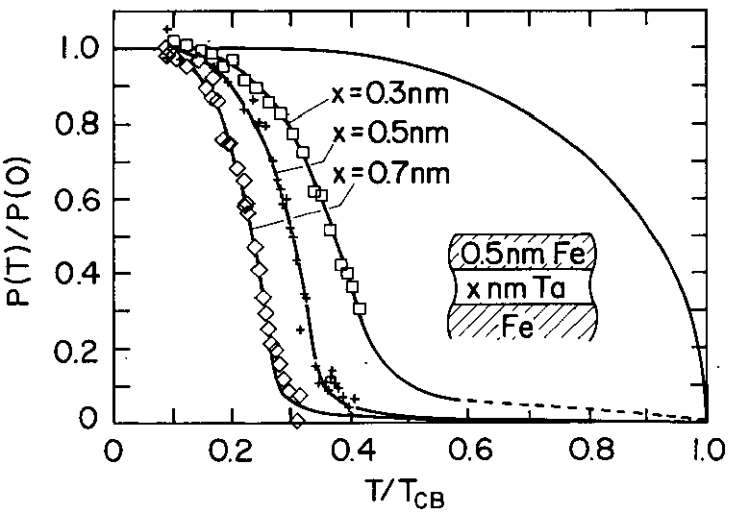

Figure 13. Relative spin polarization $P(T)/P(0)$ of the low-energy cascade electrons from the 0.5 nm polycrystalline Fe film in the ferromagnetic state for various thicknesses x of the Ta spacer. $T = T/T_{CB}$ where $T_{CB} = 1043$ K is the Curie point of bulk Fe. The solid curves are calculated from mean-field theory for $s = \frac{1}{2}$ in H_{ex} which is chosen to match the observations. The mean-field curve for bulk Fe ($H_{ex} = 0$) is shown to illustrate the crossover from 2D to 3D magnetism. From [103].

A different crossover from 2D to 3D magnetism was investigated by Li and Baberschke [106] who prepared Ni(111) films on W(110). Ni/W was chosen because the generally much lower $T_{CB} = 637$ K of 3D Ni allows one to observe the phase transition even with thicker films without interference from interdiffusion with the W substrate. The crossover occurs here as the thickness of the film increases to about 4–6 ML, and it is observed via the magnetic resonance at 9 GHz. An external magnetic field of $\sim 10^5$ A m^{-1} has to be applied parallel to the plane of the films. Therefore, one starts already with a quasi-2D system, and observes the crossover of the quasi-2D

system to 3D. The number of layers at which this transition occurs agrees with the general definition of what '2D' means in magnetism. Namely, one has to have a film which is thin enough that spin waves with wavevector perpendicular to the film plane are not excited at the temperature under consideration.

3.3. Magnetic domains in ultrathin films

For a sufficiently large 3D ferromagnetic body, the uniformly magnetized state is higher in energy than the state in which magnetic domains are present. With the domains, the energy associated with the magnetic stray fields created outside the sample can be reduced at the expense of the energy necessary to create domain walls separating two domains with different magnetization direction. If, however, the dimensions of the 3D ferromagnetic body become smaller or comparable to the width w of a domain wall, the uniformly magnetized state is more favourable in energy. Therefore, magnetic domains do not occur in 3D bodies that are small compared to w.

With ultrathin films, the situation is more complex. Everything depends on whether the easy direction of $M_0(T)$ is in the plane of the films or perpendicular to it. If M_0 is in-plane, the lowest-energy state is the homogeneously magnetized one, but if M_0 is out-of-plane, domains may be more favourable depending on the ratio ρ of the exchange energy to the dipolar energy. Yafet and Gyorgy [107] argue that domains should occur for a small range of ρ-values only, namely for $1 \leqslant \rho \leqslant 1.4$. The calculation is difficult because the action of the dipolar field on the domain wall has to be included, in contrast to the 3D case where the energy per unit surface area γ of a domain wall is simply determined by a competition between exchange energy and anisotropy energy. The exchange energy with A the exchange stiffness per unit length is minimal when the wall is very thick, whereas the anisotropy energy per volume K is minimal when the wall is very thin. The optimum occurs with $w = \sqrt{A/K}$ and $\gamma \simeq \sqrt{AK}$. With very thin films, additional relevant quantities are $\delta = w/L$ where L is the diameter of the domains, and the ratio ρ of exchange and dipolar energy [107]. It is apparent that the study of domains and particularly domain wall widths yields important information on the exchange stiffness $A_{\|}$ along a path in the plane of the film and on the surface anisotropy K_S. Defects are expected to be important for the location of domain walls, since $A_{\|}$, K_S and the dipolar energy are certainly different when, e.g., steps or holes are present.

The best technique to image magnetic domains in ultrathin films is scanning electron microscopy with polarization analysis (SEMPA) [50]. Allenspach *et al* [99] used SEMPA to investigate magnetic domains in epitaxial Co/Au(111) films. For 3 ML, the Co layer grows with the well-known sixfold symmetry characteristic of hexagonal Co(001). The tensile strain in the surface of the 3 ML film is as high as 8%, but the lattice is completely relaxed to the bulk value at 6 ML. With 3 ML at $T = 300$ K, the magnetization is perpendicular to the surface, and δ and ρ assume values that should make the state with magnetic domains more favourable according to [107]. *This is indeed what is observed* [99]. The domains are generated spontaneously and have an average diameter $L \simeq 2\mu$m. The domain wall width w is less than 20 nm; hence the internal structure of the domain walls cannot be studied as it is below the present experimental resolution. L is much larger than the average step width of the substrate of 50 nm. Even at extended irregularities in the topography of the substrate, in-plane magnetizations have not been observed. Possibly there are still

too many defects whose influence may cancel so that the exchange interaction ties all the moments to the one direction perpendicular to the film. Even by annealing, the homogeneously magnetized state could not be produced. This changes when more than 5 ML of Co are deposited: the magnetization then undergoes a smooth transition to an in-plane direction. In that case, a homogeneously magnetized state can be reached by applying briefly an external magnetic field [99]. But a state with domains is also possible. It is difficult to decide conclusively from the experiments whether the state with or without domains is lower in energy.

The finding that films with in-plane magnetization exhibit a homogeneously magnetized state is corroborated by studies on Co/Cu(001) [98]. In that case, the epitaxial Co grows as an almost perfect continuation of the substrate in the FCC (100) structure [108]. The magnetization direction is in-plane right from the first appearance of ferromagnetism with 1 ML [98].

The Co films are in a single-domain state over millimetre-sized areas, even when evaporated in a field-free space, in agreement with the expectations [107]. However, domains can be generated by demagnetizing the sample in a decreasing AC field [98, 109]. The easy axis is fourfold along the [110] directions, and the walls between the domains are of the Néel type with $w \simeq 40$ nm as the one easy direction in the middle of the wall stabilizes this configuration [98].

Berger, Linke and Oepen have studied the effects of steps in the substrate on the magnetic anisotropy of Co/Cu(001) [110]. Successive regular (001) terraces separated by monatomic steps running essentially along {110} produced uniaxial anisotropy with the easy axis of magnetization parallel to the edge of the steps. This might be attributed to the demagnetization energy for a magnetization direction perpendicular to the steps, but other explanations are also possible [110].

Altogether the existing experiments with magnetic domains confirm the theoretical expectations [107] but with the qualification that it is not straightforward to decide whether or not an observed state is stable or simply metastable. Domain walls are generally much thinner in the ultrathin films compared to the bulk, and much interesting information on primary magnetic properties is expected from the study of the inner structure of domain walls in ultrathin films.

Acknowledgments

The author gratefully acknowledges helpful discussions with collaborators and colleagues as well as generous communication of results prior to publication.

References

[1] Mathon J 1988 *Rep. Prog. Phys.* **51** 1
[2] Binder K 1983 *Phase Transitions and Critical Phenomena* vol 18, ed C Domb and J L Lebowitz (New York: Academic)
[3] Busch G, Campagna M and Siegmann H C 1970 *J. Appl. Phys.* **41** 1044
[4] Siegmann H C, Meier F, Erbudak M and Landolt M 1984 *Adv. Electron. Electrical Phys.* **62** 1; 1985 *Polarized Electrons in Surface Physics (Advanced Series in Surface Science)* ed R Feder (Singapore: World Scientific)
[5] Meyer W and Steffens E (ed) 1991 *High Energy Spin Physics* (Berlin: Springer)
[6] Siegmann H C, Mauri D, Scholl D and Kay E 1988 *J. Physique Coll.* **C8** 9–16 and references therein

[7] Borgiel W, Nolting W and Donath M 1989 *Solid State Commun.* **72** 825; Donath M, Dose V, Ertl K and Kolac V 1990 *Phys. Rev.* B **41** 5509
[8] Kisker E, Schröder K, Goudat W and Campagna M 1985 *Phys. Rev.* B **31** 329 and references therein
[9] Seah M P and Dench W A 1979 *Surf. Interface Anal.* **1** 2
[10] Taborelli M 1988 *Dissertation* ETH Zurich, No 8545
[11] Abraham D L, Hopster H 1989 *Phys. Rev. Lett.* **62** 1157
[12] Glazer J, Tosatti E 1984 *Solid State Commun.* **52** 905
[13] Venus D, Kirschner J 1988 *Phys. Rev.* B **37** 2199
[14] Gokhale M P and Mills D L 1991 *Phys. Rev. Lett.* **66** 2251
[15] Pierce D T and Siegmann H C 1975 *Phys. Rev.* B **9** 4035
[16] Donath M, Scholl D, Siegmann H C and Kay E 1991 *Appl. Phys.* A **52** 206
[17] Paul O, Toscano S, Totland K and Landolt M 1991 *Surf. Sci.* **251/252** 27; Paul O 1990 *Dissertation* ETH Zurich, No 9210
[18] Unguris J, Pierce D T and Celotta R J 1992 *Phys. Rev. Lett.* **69** 1125
[19] Pappas D P, Kämper K-P, Miller B P, Hopster H, Fowler D E, Brundle C R, Luntz A C and Shen Z X 1991 *Phys. Rev. Lett.* **66** 504
[20] Donath M, Scholl D, Mauri D and Kay E 1991 *Phys. Rev.* B **43** 13 164
[21] Donath M 1989 *Appl. Phys.* A **49** 351
[22] Wohlfarth E P 1970 *J. Appl. Phys.* **41** 1205
[23] Abraham D L and Hopster H 1987 *Phys. Rev. Lett.* **58** 1352
[24] Starke K, Ertl K and Dose V 1992 *Phys. Rev.* B
[25] Donath M, Dose V, Ertl K and Kolac U 1990 *Phys. Rev.* B **41** 5509
[26] Vaterlaus A, Milani F and Meier F 1990 *Phys. Rev. Lett.* **65** 3041
[27] Helman J S and Baltensperger W 1991 *Mod. Phys. Lett.* B **5** 1769
[28] Scholl D, Donath M, Mauri D, Kay E, Mathon J, Muniz R B and Siegmann H C 1991 *Phys. Rev.* B **43** 13 309
[29] Mathon J and Ahmad S P 1988 *Phys. Rev.* B **37** 660
[30] Mills D L and Maradudin A A 1967 *J. Phys. Chem. Solids* **28** 1855
[31] Mauri D, Scholl D, Siegmann H C and Kay E 1988 *Phys. Rev. Lett.* **61** 758
[32] Pini M G and Rettori A 1990 *Phys. Rev.* B **41** 779
[33] Bruno P and Renard J P 1989 *Appl. Phys.* A **49** 499
[34] Weber R and Tannenwald P E 1963 *J. Phys. Chem. Solids* **24** 1357
[35] Brundle C R, Silverman E and Madix R J 1979 *J. Vac. Sci. Technol.* **16** 4741
[36] Mamaev Yu A, Petrov V N and Starovoitov S A 1987 *Sov. Tech. Phys. Lett.* **13** 642
[37] Crangle J and Hallam G C 1963 *Proc. R. Soc.* A **272** 119
[38] Alvarado S F, Campagna M and Hopster H 1982 *Phys. Rev. Lett.* **48** 51
[39] Taborelli M, Paul O, Züger O and Landolt M 1988 *J. Physique Coll.* **49** C8 1569
[40] Rau C and Robert M 1987 *Phys. Rev. Lett.* **58** 2714
[41] Weller D, Alvarado S F, Goudat W, Schroeder K and Campagna M 1985 *Phys. Rev. Lett.* **54** 1555
[42] Farle M and Baberschke K 1987 *Phys. Rev. Lett.* **58** 2714
[43] Sanches J M and Moran-Lopez J L 1987 *Surf. Sci.* **58** 1120; 1988 *Surf. Sci.* **198** 299
[44] Weller D and Alvarado S F 1988 *Phys. Rev.* B **37** 9911
[45] Rau C, Jin C and Robert M 1988 *J. Appl. Phys.* **63** 3667
[46] Dauth B H, Alvarado S F and Campagna M 1987 *Phys. Rev. Lett.* **58** 2118
[47] Diehl H W and Hüsser A 1986 *Phys. Rev. Lett.* **56** 2834
[48] Friedberg R and Paul D I 1975 *Phys. Rev. Lett.* **34** 1234
[49] Zijlstra Hinne 1979 *IEEE Trans. Magn.* **MAG-15** 1246
[50] Scheinfein M R, Unguris J, Kelley M H, Pierce D T and Celotta R J 1990 *Rev. Sci. Instrum.* **61** 2501 and references therein
[51] Scheinfein M R, Unguris J, Blue J L, Coakley K J, Pierce D T and Celotta R J 1991 *Phys. Rev.* B **43** 3395 and references therein
[52] Aeschlimann M, Scheinfein M, Unguris J, Greidanus F J A M and Klahn S 1990 *J. Appl. Phys.* **68** 4710 and references therein
[53] Sattler K and Siegmann H C 1972 *Phys. Rev. Lett.* **29** 1565
[54] Siegmann H C and Bagus P S 1988 *Phys. Rev.* B **38** 10 434
[55] Siegmann H C, Bagus P S and Kay E 1988 *Z. Phys.* B **69** 485
[56] Gay J G and Richter R 1986 *Phys. Rev. Lett.* **56** 2728
[57] Oepen H P and Kirschner J 1989 *Phys. Rev. Lett.* **62** 819

[58] Rave W, Schäfer R and Hubert A 1987 *J. Magn. Magn. Mater.* **65** 7 and references therein
[59] Bona G L, Meier F, Schönhense G, Aeschlimann M, Stampanoni M, Zampieri G and Siegmann H C 1986 *Phys. Rev.* B **34** 7784
[60] Aeschlimann M, Vaterlaus A, Lutz M, Stampanoni M, Meier F, Siegmann H C, Klahn S and Hansen P 1991 *Appl. Phys. Lett.* **59** 2189
[61] Vaterlaus A, Guarisco D, Lutz M, Aeschlimann M and Meier F 1990 *J. Appl. Phys.* **67** 5661
[62] Vaterlaus A, Beutler T and Meier F 1991 *Phys. Rev. Lett.* **67** 3314
Vaterlaus A, Beutler T, Guarisco H, Lutz M and Meier F 1992 *Phys. Rev.* B **46** 5280
[63] Neugebauer C A 1962 *Phys. Rev.* **116** 1441
[64] Gradmann V 1974 *Appl. Phys.* **3** 161
[65] Herring C and Kittel C 1951 *Phys. Rev.* **81** 869
Mermin M D and Wagner H 1966 *Phys. Rev. Lett.* **17** 1133
[66] Blügel S 1992 *Phys. Rev. Lett.* **68** 851
[67] Fu C L, Freeman A J and Oguchi T 1985 *Phys. Rev. Lett.* **54** 2700
[68] Ericson D, Albers R C and Boring A M 1991 *Phys. Rev. Lett.* **66** 1350
[69] Bader S D 1991 *J. Magn. Magn. Mater.* **100** 440
[70] Rau C, Xing G, Liu C and Robert M 1989 *Phys. Lett.* **135A** 227
[71] Stampanoni M, Vaterlaus A, Pescia D, Aeschlimann M, Dürr W and Blügel S 1988 *Phys. Rev.* B **37** 10 380
[72] Freeman A J and Fu C L 1987 *J. Appl. Phys.* **61** 3356
[73] Landskron H, Schmidt G, Heinz K, Müller K, Stuhlmann C, Beckers U, Wuttig M and Ibach H 1991 *Surf. Sci.* **256** 115
[74] Kerkmann D, Pescia D, Krewer J W and Vescove E 1991 *Z. Phys.* B **85** 311
[75] Schneider C M, Bressler P, Schuster D, Kirschner J, de Miguel J J, Miranda R 1990 *Phys. Rev. Lett.* **64** 1059
[76] Krakauer H, Posternak M and Freeman A J 1979 *Phys. Rev.* B **19** 1709
[77] Jepsen O, Madsen J and Andersen O K 1980 *J. Magn. Magn. Mater.* **15–18** 867
[78] Lugert G and Bayreuther G 1992 *Preprint*
[79] Xhonneux P and Courtens E 1992 *Phys. Rev.* B **46** 556
Xhonneux P 1992 *Dissertation* ETH Zurich, No 9797
[80] Macedo W A A and Kenne W 1988 *Phys. Rev. Lett.* **61** 475
[81] Pescia D, Stampanoni M, Bona G L, Vaterlaus A, Willis R F and Meier F 1987 *Phys. Rev. Lett.* **58** 2126
Stampanoni M 1989 *Appl. Phys.* A **49** 449; 1989 *Dissertation* ETH Zurich, No 8937
[82] Pappas D P, Kämper K P and Hopster H 1990 *Phys. Rev. Lett.* **64** 3179
[83] Liu C, Moog E R and Bader S D 1988 *Phys. Rev. Lett.* **60** 2422
[84] Bennett W R, Schwarzacher W and Egelhoff W F Jr 1990 *Phys. Rev. Lett.* **65** 3169
[85] Dutscher J R, Heinrich B, Cochran J F, Steigerwald D A and Egelhoff W F Jr 1988 *J. Appl. Phys.* **63** 3464
[86] Celinsky Z and Heinrich B 1991 *J. Appl. Phys.* **70** 5935
[87] Stampanoni M and Allenspach R 1992 *J. Magn. Magn. Mater.* **104–107** 1805
[88] Pokrovsky V 1979 *Adv. Phys.* **28** 595
[89] Morrish A H 1965 *The Physical Principles of Magnetism* (New York: Wiley) p 360
[90] Néel L 1954 *J. Physique Radium* **15** 225
[91] Mauri D, Scholl D, Siegmann H C and Kay E 1989 *Appl. Phys.* A **49** 439
[92] Dürr W, Taborelli M, Paul O, Germer R, Goudat W, Pescia D and Landolt M 1989 *Phys. Rev. Lett.* **62** 206
[93] Qiu Z Q, Pearson J and Bader S D 1991 *Phys. Rev. Lett.* **67** 1646
[94] Doring W 1991 *Z. Naturf.* a **16** 1146
[95] Pini H G, Rettori A, Pescia D, Maglis N and Selzer S 1992 *Phys. Rev.* B **45** 5037
[96] Mauri D, Scholl D, Siegmann H C and Kay E 1989 *Phys. Rev. Lett.* **62** 1900
[97] Weber W, Kerkmann D, Pescia D, Wesner D A and Güntherodt G 1990 *Phys. Rev. Lett.* **65** 2058
[98] Kerkmann D, Pescia D and Allenspach R 1992 *Phys. Rev. Lett.* **68** 686
[99] Allenspach R, Stampanoni M and Bischof A 1990 *Phys. Rev. Lett.* **65** 3344
[100] Pescia D and Pokrovsky V L 1990 *Phys. Rev. Lett.* **65** 2599
[101] de Jongh J and Miedema A R 1974 *Experiments on Simple Magnetic Model Systems* (London: Taylor & Francis)

[102] Kosterlitz J M and Thouless D J 1978 *Progress in Low Temperature Physics* vol VII B (Amsterdam: North-Holland)
[103] Donath M, Scholl D, Siegmann H C and Kay E 1991 *Phys. Rev.* B **43** 3164
[104] Hirakawa K and Ubukoshi K 1981 *J. Phys. Soc. Japan* **50** 1909
[105] Egelhoff W F Jr and Steigerwald D A 1989 *J. Vac. Sci. Technol.* A **7** 2167
[106] Li Yi and Baberschke K 1992 *Phys. Rev. Lett.* **68** 1208
[107] Yafet Y and Gyorgy E M 1988 *Phys. Rev.* B **38** 9145
[108] Schmid A 1992 *Dissertation* FU Berlin and references therein
[109] Oepen H P, Benning M, Ibach H, Schneider C M and Kirschner J 1990 *J. Magn. Magn. Mater.* **86** L137
[110] Berger A, Linke U and Oepen H P 1992 *Phys. Rev. Lett.* **68** 839